Doctoral Dissertation (Censored)

博士論文 (要約)

A study of the hierarchical structure in the Antarctic atmosphere based on PANSY radar observations and high-resolution general circulation model simulations

(PANSY レーダー観測と高解像度大気大循環モデル再現実験に基づく南極大気の階層構造の研究)

A Dissertation Submitted for the Degree of Doctor of Philosophy

December 2021

令和３年１２月博士（理学）申請

Department of Earth and Planetary Science,
Graduate School of Science, The University of Tokyo
東京大学 大学院理学系研究科 地球惑星科学専攻

Yuichi Minamihara
南 原　優 一

Abstract

It is well known that atmospheric Rossby waves (RWs) and gravity waves (GWs) excited mainly in the troposphere, propagate upward, and drive the general circulation in the middle atmosphere by transporting momentum. The momentum transports by GWs and RWs have conventionally been investigated separately. However, several studies using a high-resolution general circulation model (GCM) that explicitly resolves GWs have reported that GWs are radiated from a distorted RW in the stratosphere. Furthermore, studies using a high-top GCM permitting GWs which covers from the ground to the upper mesosphere and above have shown that in-situ RW generation in barotropic and/or baroclinic instability is maintained by the GW forcing in the mesosphere. Thus, we have glimpsed the interplay between RWs and GWs, which is a part of relations between atmospheric phenomena having different temporal and spatial scales within a hierarchical structure of the middle atmosphere including RWs and GWs. A few studies have attempted to elucidate the hierarchical structure of the atmosphere composed of various phenomena having different scales.

Recent studies that compared satellite observations and GCM simulations suggested that GWs generated around the Antarctica significantly contribute to the middle-atmosphere general circulation, but the observation of the Antarctic atmosphere was a challenge due to the harsh environment. In, 2011, the Program of the Antarctic Syowa (PANSY) radar, which is the first Mesosphere-Stratosphere-Troposphere/Incoherent Scatter (MST/IS) radar in the Antarctic, was installed at Syowa Station (69.0°S, 39.6°E) and it enables to examine RWs and GWs in the Antarctic regions using direct measurements with a fine vertical resolution. The purpose of this study is to elucidate the hierarchical structure in the Antarctic atmosphere over broad spatial and temporal ranges from Kelvin-Helmholtz (KH) billows to the polar vortex, based on the observations by the PANSY radar and radiosondes with high accuracy and resolution at Syowa Station as well as numerical

simulations using GW-permitting GCMs. In particular, this study focuses on the atmospheric phenomena observed at Syowa Station during the observational campaigns performed in 2019.

In Chapter 2, we focus on the dynamical relations among relatively small-scale phenomena from KH billows to synoptic-scale waves. During 14–24 March and 2–12 August 2019, observation campaigns targeting atmospheric turbulence in the troposphere and lower-stratosphere were performed using the PANSY radar and radiosondes. The PANSY radar performed the observation with the frequency radar interferometric imaging technique, which provides the data with high resolutions in time and range. A total of 73 'S-shaped' structures, which are characteristic of KH billows, were detected in the time-height section of echo power during the campaigns. Numerical simulations using the Non-hydrostatic Icosahedral Atmospheric Model (NICAM) were also carried out in order to investigate the spatial structure of the atmospheric phenomena related to the generation of the observed KH billows in these periods.

First, a detailed analysis for the observed KH billows was performed. Since the height and time regions where clear KH billow structures were found were limited, we focused on two representative examples out of all observed KH billows. The first case is the KH billow with the longest duration, likely excited by a strong vertical shear associated with orographic GWs according to the analysis based on the observation as well as the NICAM simulations. The theoretically infinite wave periods and steadily maintained phase structure of orographic GWs are consistent with the long duration of this KH billow. The second case is the KH billow with the deepest vertical structure. The KH instability of this case was likely caused by upper-tropospheric jet associated with a cyclone. These results indicate that there are at least two excitation mechanisms of KH billows in the Antarctic region. These two excitation mechanisms reflect the characteristics in the Antarctic: steep coastal topography and well-developed synoptic-scale cyclones.

We also examined the most unstable modes expected from a two-dimensional linear

stability theory applied for the idealized background field of the two cases mentioned above. The most unstable modes have horizontal wavelengths and depths that roughly match those of observed KH billows. These results suggests that the observed KH billows are consistent with the maximum growth mode expected from linear stability theory.

This study also showed the dynamical statistical characteristics of KH billows in the Antarctic for the first time. The mean and probability density function of the horizontal wavelength, thickness, and aspect ratio of all 73 observed KH billows waves are almost the same as those estimated by the mid-latitude observations. It means that the dynamical properties of KH billows in the Antarctic are found to be similar to those in mid-latitudes. On the other hand, the magnitude of vertical shear of the background wind is about 60 % of that estimated at mid-latitudes. Moreover, the wave period of the KH billows is about twice as long as that at mid-latitudes. This result probably likely reflects that the tropospheric jets over the Syowa Station are not as strong as those over Japan.

In Chapter 3, we focused on the dynamical relations among relatively large-scale phenomena from GWs to the polar vortex. Specifically, we examined the time evolution of the dynamical properties of GWs and RWs during the Southern Hemisphere stratospheric sudden warming in September 2019 (SSW-SH 2019). Simultaneous measurements using the PANSY radar and radiosondes were made from 26 August to 2 October 2019, targeting disturbances in the lower stratosphere during the SSW-SH 2019. In addition, short numerical simulations using a high-resolution (T639L340) Japanese Atmospheric General circulation model for Upper Atmosphere Research (JAGUAR) were performed to investigate the dynamical properties of GWs and RWs especially quasi-6-day waves (Q6DWs) below the lower thermosphere. Some previous studies reported that Q6DWs in the mesosphere and above were enhanced during the SSW-SH 2019.

First, using the PANSY radar and radiosonde observation data, the high-resolution JAGUAR simulations were verified. It was shown that the high-resolution JAGUAR reproduced

GWs in the lower stratosphere well, but the amplitude of the simulated vertical wind disturbances associated with the GWs was about one-fifth of that observed.

Next, we examined the spatial distribution and time variation of GWs during the SSW-SH 2019. We found large negative momentum fluxes associated with GWs in the stratosphere above the Andean Mountains and the Antarctic Peninsula before the SSW onset (7 September) and above and leeward of the Ross Sea after the onset. On the other hand, in the mesosphere (especially above $z =$ 75 km), largely negative momentum flux was observed to the south of 40°S before 3 September. During 3–10 September when the polar vortex became obscure, positive momentum flux was seen around 60°S. After 10 September when the polar vortex reappeared, negative momentum flux was observed again to the south of 40°S, although its magnitude was smaller than that before 3 September.

We also investigated the dynamical characteristics of Q6DWs using the JAGUAR-Data Assimilation System (JAGUAR-DAS) analysis data and high-resolution JAGUAR simulations for SSW-SH 2019. The JAGUAR-DAS analysis data which can be used for analysis of waves with low wavenumbers enable us to analyze RWs for longer time periods. There were two types of Q6DWs, one with eastward phase velocity (Q6DW-E) and the other with westward phase velocity (Q6DW-W). It was found that Q6DW-Es were dominant to the south of 50°S before 10 September, and Q6DW-Ws were dominant in both hemispheres after that in the mesosphere. The Q6DW-E and Q6DW-W have a baroclinic structure in the vertical, which is different from a barotropic structure of normal mode 5-day Rossby wave.

Excitation mechanisms of the Q6DW-E and Q6DW-W were investigated in terms of Eliassen-Palm fluxes (EP fluxes) and modified potential vorticity (MPV). It was suggested that the Q6DW-E is an unstable wave due to baroclinic-instability, which is conditioned by a pair of the meridional gradient of MPV: a negative gradient in high-latitude mesosphere and a positive gradient in the stratosphere. This inference is supported by the fact that the Q6DW-E was no longer observed

after the negative MPV gradient in the mesosphere disappeared. On the other hand, the Q6DW-W is likely to be an internal RW generated from barotropic/baroclinic instability in the upper stratosphere over 60°–80°S. This dynamical instability was associated with the MPV maximum due to the maximum of the static stability broadly existing over 40°–70°S in the upper stratosphere. We showed that the static stability maximum was caused by a downward residual flow from $z =$ 50 km at 80°S to $z = 70$ km at 40°S. This downward residual flow was partly driven by a combination of the positive RW forcing (eastward acceleration) expanding from $z = 50$–80 km at 80°S to $z = 70$ km at 40°S due to the Q6DW-E and the negative wave forcing (westward acceleration) in the region from $z < 50$ km at 80°S to $z < 60$ km at 40°S due to the convergence of RWs propagating from the mid- and high-latitudes troposphere. In addition, a pair of the positive GW forcing in the polar mesosphere and the negative GW forcing in the stratosphere contribute similarly to the downward residual flow at almost the same magnitude. It was also suggested that the Q6DW-W originated from the Southern Hemisphere and spread the Northern Hemisphere. We suggested that the positive GW forcing in the region where the polar vortex shifted to the lower latitudes due to the SSW play an important role in the excitation of Q6DW-W in September 2019. This is consistent with the most obvious dominance of Q6DW-W in September 2019 during 2015 and 2020.

In this thesis, we examine the relations between phenomena with different scales in the atmospheric hierarchy structure. In the first half, we suggested that orographic GWs and cyclones having the enhanced upper-tropospheric jets likely excited KH billows in the Antarctic coastal region. They are characteristic phenomena in the Antarctic coastal region. In the second half, we confirmed that RW and GW forcings weakened the polar vortex and eventually led to the SSW-SH 2019. We also showed how the GW distribution varies with the shift of the polar vortex during the SSW-SH 2019. For Q6DWs, we indicated that the mesospheric RW and GW forcings contribute to the excitation of Q6DW-E and that the Q6DW-E forcing and the GW forcing distribution associated with

the shifted polar vortex likely contributed to the excitation of internal RWs, namely Q6DW-W, from the barotropic and/or baroclinic instability. However, the relations among atmospheric phenomena with different temporal and spatial scales shown in this study are only a part of the hierarchical structure in the Antarctic atmosphere. More studies based on both high-resolution observations and numerical simulations utilizing GW-permitting GCMs are necessary to understand the hierarchical structure further. By extending the analysis period longer, it will be possible to examine seasonal and year-to-year variations in the relationships within the hierarchical structure.

In particular, an accumulation of case studies is essential for elucidating whether there are other new excitation mechanisms of KH billows and for statistical significance for the mean values and probability density function of characteristics of KH billows in the Antarctic. It is also interesting to confirm the robustness of the excitation mechanism of Q6DW shown in this study. The examination of the interannual variation of Q6DW is necessary in terms of the Q6DW-E and GW forcing, which are a key for the excitation mechanism of Q6DW-W. The investigation what determines the time lag between the appearance of the barotropic/baroclinic instability and the onset of Q6DW-W dominance is also future work.

要旨

主に対流圏で励起されたロスビー波と重力波は、対流圏から運動量を運び中層大気の大気大循環を駆動していることが知られている。これまで、スケールの異なる重力波とロスビー波の運動量輸送は別々に議論されることが多かった。しかし、重力波を解像する大気大循環モデルを用いた一連の研究は、重力波が成層圏のゆがんだロスビー波から放射される様子を報告している。また、下部熱圏まで解像するハイトップかつ高解像度な大気大循環モデルを用いた研究は、重力波が形成した中間圏の不安定な場からロスビー波が発生することを示している。このように、ロスビー波と重力波がダイナミックに相互作用する階層構造の存在が垣間見られている。一方、衛星観測と気候モデル実験から重力波の運動量フラックスの緯度分布を比較した研究から、中層大気大循環における南極域の重力波の役割は極めて大きいことが予想されている。しかし、スケールの異なる大気現象間の相互関係を含めた、大気の階層構造を包括的に理解しようとする研究は少ない。さらに、南極域はその過酷な環境故に観測が不足しており研究が遅れている。本研究の目的は、南極昭和基地 (69.0°S, 39.6°E) に設置された PANSY レーダーの高精度・高分解能な観測と、重力波を陽に解像する高解像度大循環モデルの再現実験の両方に基づいて、Kelvin-Helmholtz (KH) 波から極渦までの広い時空間スケールに亘る、南極大気の階層構造を定量的に理解することである。特に本論文では、2019 年に昭和基地にて行われた観測キャンペーンにて捉えられた大気現象に着目する。

第 2 章では、KH 波から総観規模波動に亘る南極大気の階層構造のうち、比較的小スケールの現象間の力学的関係に着目した。2019 年 3 月 14 日から 24 日、8 月 2 日から 12 日に対流圏と下部成層圏の大気乱流をターゲットとした PANSY レーダーとラジオゾンデを同期した観測キャンペーンを計 20 日間実施した。特に PANSY レーダーの周波数領域

干渉計法 (FII) モードを用いた観測を行い、時間方向と高度方向に高解像度な鉛直風とエコー強度のデータを取得した。この期間中、エコー強度の時間高度断面から、KH 波に特徴的な S 字型構造が目視で 73 例検出された。また、KH 波をもたらしたと考えられる大気現象の空間構造を調べるために、非静力学正 20 面体格子大気モデル (NICAM) を用いた再現実験も併せて実施した。

まず、全事例の中で特に特徴的な構造を持っていた 2 つの KH 波について事例解析を行った。最も継続時間が長かった KH 波 (Case A) は地形性重力波に伴う強い鉛直シアによって励起された可能性が高いことが分かった。Case A の継続時間が長いことは、地形性重力波の周期が理論上無限であることと地形性重力波の鉛直位相構造が定常であることと整合的である。一方、最も鉛直方向に深い構造を有していた KH 波 (Case B) は、発達した低気圧に伴う上部対流圏のジェットによって励起された可能性が高いことが NICAM 再現実験の結果から分かった。以上から、南極域の KH 波には少なくとも 2 つの励起メカニズムがあることが明らかになった。地形性重力波と発達した低気圧は南極域において特徴的な大気現象であることが知られている。

次に、線形安定性理論から求められた最も不安定なモードを調べたところ、事例解析で着目した KH 波とよく似た性質が求められた。また、本研究は、南極域の KH 波の力学的特徴をはじめて統計的に示した。統計解析からは、KH 波の波長、厚み、縦横比の値は、中緯度における観測値とほぼ同じであることが分かった。一方、背景風の鉛直シアの強さは中緯度観測の 60 % 程で、KH 波の周期は中緯度における観測の約 2 倍であった。これは、昭和基地上空の対流圏ジェットが日本上空の対流圏ジェットと比べて弱いことを反映した結果だと考えられる。

第 3 章では、重力波から極渦に亘る、南極大気の階層構造のうち比較的大スケー

ルの現象間の関係に着目した。特に、2019 年 9 月に発生した南半球成層圏突然昇温中の重力波とロスビー波の力学的特性の時間変化に着目した。突然昇温中の 2019 年 8 月 26 日から 10 月 2 日にかけて、昭和基地では、成層圏突然昇温中の下部成層圏擾乱を観測ターゲットとした、PANSY レーダーとラジオゾンデの同時観測キャンペーンを実施した。また、重力波とロスビー波、特に準 6 日波 (Q6DW) の力学的特性の時間変化を調べるために、高解像度 JAGUAR (T639L340) を用いた地表面から下部熱圏まで解像する数値再現実験も併せて実施した。

PANSY レーダーとラジオゾンデの観測データを用いて、高解像度 JAGUAR の再現実験を検証したところ、高解像度 JAGUAR は重力波と思われる下部成層圏の波型構造をよく再現していることが分かった。一方で、高解像度 JAGUAR の重力波の鉛直風擾乱の振幅は、現実大気の重力波の 1/5 程度であることが示された。また、昭和基地上空の重力波は西半球にシフトした極渦の縁が昭和基地上空に接近した時に活発になることがわかった。

南極域の重力波の分布に着目した解析を行ったところ、成層圏突然昇温前にはアンデス山脈と南極半島上空で、成層圏突然昇温後には高緯度のロス海上空とその風下で、成層圏の重力波活動が活発であることがわかった。一方、高度 75 km 以上では、成層圏突然昇温前極渦は強く、大きな負の東西運動量鉛直フラックスが南緯 40 度以南に分布していたのに対して、9 月 3 日から 10 日には、極渦は消失し正の運動量フラックスが南緯 60 度付近に現れ、その絶対値は小さかった。9 月 11 日以降、再び極渦が現れ、負の運動量フラックスが南緯 40 度以南に現れるが、その大きさは突然昇温前よりも小さかった。

次に、JAGUAR-Data Assimilation System (JAGUAR-DAS) 解析データと高解像度 JAGUAR データを用いて、準 6 日波 (Q6DW) の力学的特徴を調べた。JAGUAR-DAS 解析

データは、ロスビー波の解析には使用可能な解像度を有している。今回は長期間の Q6DW を解析するために JAGUAR-DAS 解析データを使用した。突然昇温中の Q6DW には東向位相速度成分 (Q6DW-E) と西向き位相速度成分 (Q6DW-E) の両方が存在していたことが分かった。また、突然昇温前は Q6DW-E が、突然昇温後は Q6DW-W が南極域の中間圏以上で卓越していた。さらに、Q6DW-E と Q6DW-W は傾圧的な構造を有しており、ノーマルモードの 5 日波の順圧的な構造とは異なっていた。

両 Q6DW の励起メカニズムにも着目したところ、Q6DW-E は 9 月 1 日から 6 日の南極の高度 80 km から南緯 40 度の高度 60km に伸びる負の南北渦位勾配と、南緯 40 度から南緯 80 度の高度 30 km 付近に存在する正の南北渦位勾配の対と対応する傾圧不安定波である可能性が高いことが分かった。これは、Q6DW-E が見られなくなった 9 月 10 日以降、中間圏の負の南北渦位勾配が消失していたことと整合する。 一方 Q6DW-W は、9 月 10 日から 15 日に南緯 50 度から南緯 70 度、高度 40–60 km に存在した順圧・傾圧不安定から発生した内部ロスビー波である可能性が高いことが分かった。この順圧・傾圧不安定は、同時期の高度 40–50 km の南緯 40 度から南緯 70 度にわたって広く分布していた成層安定度の極大に伴う渦位の極大によって形成されていた。成層安定度の極大は、9 月 7 日から 12 日の南緯 80 度の高度 50 km から南緯 40 度の高度 70km に亘って存在する下向きの残差流がもたらしていたと考えられる。この下向きの残差流は、Q6DW-E に伴う正の波強制と、対流圏から伝播したロスビー波の収束に伴う負の波強制が駆動していた。さらに、突然昇温後、極渦が消失した南緯 80 度の高度 50 km 以上から南緯 40 度の高度 70 km にかけて分布する正の重力波の波強制と、極夜ジェットがまだ存在している南緯 80 度の高度 40 km 以下から南緯 40 度の高度 60 km にかけて広がる負の重力波の波強制も、ロスビー波の波強制と同程度の大きさを持ち、下向きの循環の形成に大きな役割を果たしていたことが分か

った。

本研究ではいくつかのスケールの異なる大気現象間の相互関係を示した。第二章では、KH 波が地形性重力波や上部対流圏ジェットを伴う総観規模の低気圧によって励起されることを示した。地形性重力波の卓越と南極大陸に接近する低気圧に伴う強化されたジェットは南極沿岸域で特徴的な現象であることが知られている。第三章では、ロスビー波と重力波の強制が極渦を弱化し、成層圏突然昇温をもたらしたことを確認した。また、極渦の低緯度側へのシフトに伴って、重力波が活発な領域が変化し、運動量フラックスの大きさだけでなく符号も変化することも明らかにした。また、南極域中間圏のロスビー波と重力波の波強制が、Q6DW-E の励起に重要な役割を果たすことを示した。さらに、Q6DW-W の励起には、Q6DW-E に伴う南極域の正と負の波強制と、中・高緯度の対流圏から伝播するロスビー波の砕波に伴う負の波強制の他に、極域成層圏の負の重力波波強制と極域中間圏の正の重力波強制が重要であることを示した。

本研究が示したスケールの異なる大気現象間の相互関係は、南極大気の階層構造の一部に過ぎない。さらなる南極大気の階層構造の理解のためには、観測とモデル再現実験の両方を用いた多角的な研究を積み重ねる必要がある。さらに、階層構造の季節変動や年々変動を解明するには、さらに解析期間を広げた研究が必要である。

新たな KH 波の励起メカニズムの解明、より統計的に有意な KH 波の力学的特性の定量的な理解には、事例解析の積み重ねが不可欠である。また、PANSY レーダー観測から推定された乱流の鉛直拡散係数と大気大循環モデル内の乱流パラメータの空間分布の比較は、大気大循環モデル内の自由大気中の乱流スキームの発展に大きく貢献すると考えられる。さらに、本研究で示された Q6DW の励起メカニズムの検証には、Q6DW の年々変動の解析が必要であると考える。特に、Q6DW-W の励起に重要であると考えられる

Q6DW-E に伴う波強制と、弱化した極渦に伴う極域中間圏の正の重力波強制については、年々変動も含めたより詳しい定量的な解析が今後求められる。順圧/傾圧不安定が出現してから Q6DW-W が卓越するまでのタイムラグの長さについての解釈も今後の課題である。

250

Contents

Chapter 1. General Introduction

1.1 General circulation in the middle atmosphere

It is well known that synoptic-scale Rossby waves (RWs), planetary-scale RWs, and gravity waves (GWs) propagating upward from the lower atmosphere, having different spatial and temporal scales, deposit momentum in the mean field at various height and latitude regions through their dissipation and breaking processes. The wave forcing drives the material circulation in the middle atmosphere. Figure 1.1 shows a schematic illustration of each dominant wave forcing and the residual mean circulation, which is a good approximate of Lagrangian mean circulation, in the middle atmosphere (Plumb, 2002).

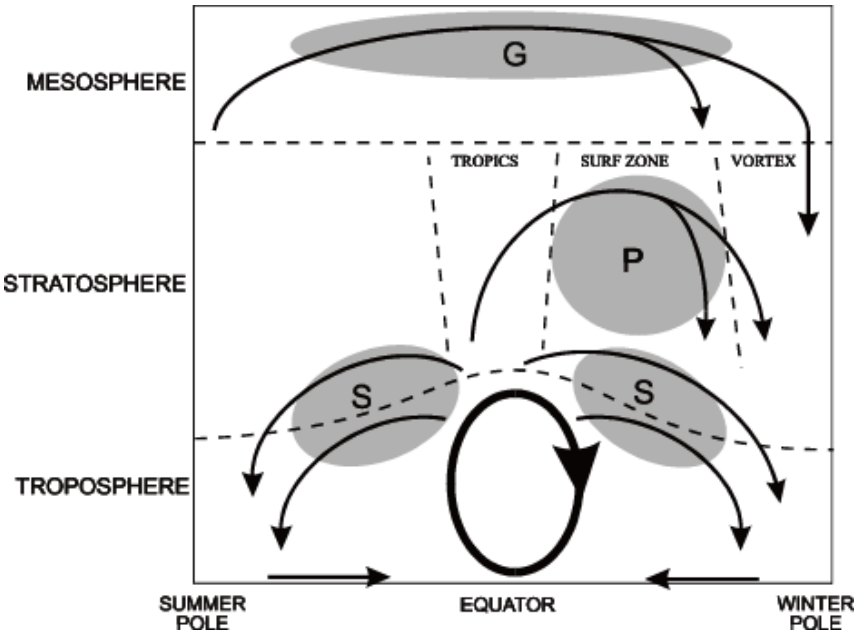

Figure 1.1: A schematic illustration of the prevailing wave forcing (shade) and the residual mean meridional circulation (arrow) in the atmosphere. The heavy ellipse denotes the thermally-driven Hadley circulation of the troposphere. Synoptic-scale Rossby waves, planetary-scale Rossby waves, and Gravity waves are labeled as "S", "P", and "G", respectively. This figure is adapted from Plumb (2002).

The global atmospheric circulation pattern of tropical tropospheric air rising into the stratosphere and then moving poleward and downward is referred to as Brewer–Dobson circulation (BDC). The synoptic-scale RWs have negative wave forcing just above the subtropical jet (Lin & Fu, 2013) and are not able to propagate deep into the stratosphere (Charney & Drazin, 1961). Thus, the synoptic-scale RW forcing drives poleward circulation in the subtropical upper troposphere and lower stratosphere in the summer and winter hemispheres. This circulation is called shallow branches of the BDC (e.g., Birner & Bönisch, 2011; Butchart, 2014). On the other hand, planetary-scale RWs break in the middle stratosphere and drive a single poleward flow in the winter hemisphere, extending to the middle and upper stratosphere. This circulation is called the deep branch of the BDC (e.g., Birner & Bönisch, 2011). Because the stationary RWs cannot propagate into the summer stratosphere where the zonal mean zonal wind is easterly (Charney & Drazin, 1961), the deep branch is not present in the summer season. In the upper mesosphere, small-scale GWs from the troposphere break and deposit the momentum. The GW forcing deaccelerates the upper part of the winter westerly jet and the summer easterly jet and maintain a weak wind layer around a height (z) of 90 km. The GW forcing also drives the residual mean meridional circulation from the summer pole to the winter pole in the mesosphere (e.g., Holton, 1983).

Adiabatic heating (cooling) induced by the downward (upward) residual mean flow provides the warm winter pole in the stratosphere and mesosphere (the cold summer pole around the mesopause). The temperature fields maintained by the adiabatic heating and cooling much differ from those expected from the radiative equilibrium. Moreover, planetary-scale RWs propagating up from the troposphere with large amplitude often give a strong westward wave forcing in the winter middle stratosphere. The wave forcing drives a strong poleward residual mean flow, and causes a strong downward residual mean flow in the polar region associating with a sudden increase in temperature.

The events with particularly drastic temperature increases (usually > 30–40 K in a matter of days) and deceleration of westerly jet through the thermal wind balance can be classified as a stratospheric sudden warming (SSW). Details of the SSW, including the definition of the SSW, are given in Chapter 3.1.

RWs owe their existence to a horizontal gradient of potential vorticity (PV) in the fluid. A common PV gradient is the β-effect (e.g., Grose & Hoskins, 1979). Large-scale orography, thermal forcing, and anomalous sea surface temperature are known to be primary sources of planetary-scale low-frequency waves (e.g., Hoskins & Karoly, 1981). They are ubiquitous in the atmosphere (Vallis, 2017). On the other hand, GWs have sources in flow over small-scale topography, convection, and jet imbalance (e.g., Alexander et al., 2010). A linear theory indicates that the intrinsic frequencies of GWs are higher than the inertial frequency, which depends on the latitude where the waves are located. The horizontal scales of GWs widely range from a few kilometers to more than a thousand kilometers (e.g., Fritts & Alexander, 2003). In the real atmosphere, many studies have reported that the excitation of GWs does not occur continuously or uniformly (intermittently). The intermittency of GWs predominantly affects the vertical profiles of GW momentum flux convergence (i.e., wave forcing to the mean wind) (Plougonven et al., 2013; Alexander et al., 2016; Hertzog et al., 2012; Minamihara et al., 2020). For example, sporadic GWs with large amplitudes tend to break and deposit the momentum on the background flow at lower heights than continuous GWs with smaller amplitudes even though they are associated with the same mean momentum fluxes (e.g., Andrews et al., 1987).

1.2 Hierarchical structures in the Antarctic atmosphere

GWs and RWs do not act independently but also interact with each other. Sato & Nomoto (2015) showed the interplay of GWs and RWs in the middle atmosphere. They indicated in-situ RW

generation from the barotropic or/and baroclinic instability. This instability is caused by a PV maximum generated by GW forcing. This RW generation causes positive and negative forcing in order to eliminate the PV maximum.

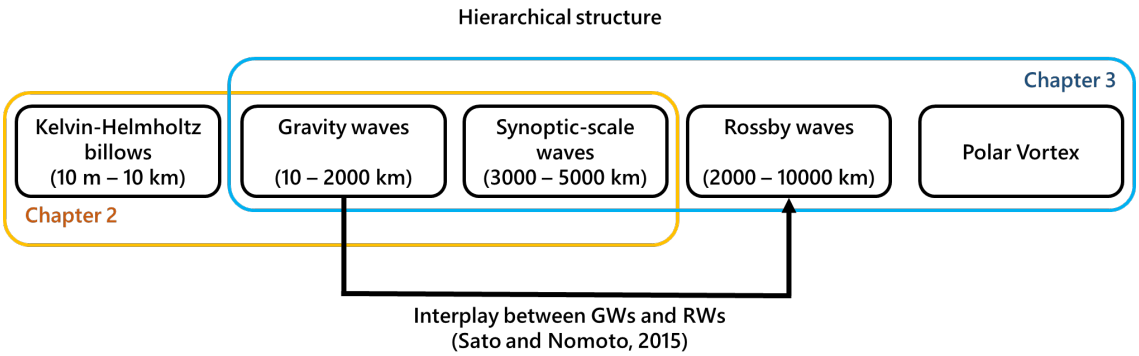

Figure 1.2: A schematic diagram of the hierarchical structures of the atmosphere. Each block shows the name and horizontal scale of each phenomenon. The black arrow indicates the interplay between GWs and RWs suggested by Sato & Nomoto (2015). The orange and blue boxes indicate the parts of the hierarchical structure that we will focus on in Chapter 2 and Chapter 3, respectively.

Previous studies also indicated that GW forcing affects the summer hemispheric part of the winter deep branch and the low-latitude part of shallow branches of the BDC (e.g., Okamoto et al., 2011; Seviour et al., 2012). Moreover, Sato & Hirano (2019) showed that GWs contribute to a higher-latitude extension of the deep branch of the BDC in all seasons except for summer using modern data-assimilation systems. This GW contribution is essential to determine the location of the turn-around latitude of the BDC. These results imply that not only RWs but also GWs form and determine the BDC in the stratosphere.

As mentioned above, there is a glimpse of the existence of a relationship within the hierarchical structure where GWs and RWs with different scales interact dynamically. In addition, the atmospheric hierarchy structure includes not only GWs and RWs but also atmospheric phenomena

with broader spatial and temporal scales, such as KH billows, synoptic-scale waves, polar vortexes, and the BDC. The relationships among atmospheric phenomena with different scales within the hierarchical structure have not been fully understood (Figure 1.2).

KH billows are generated by a shear instability called the Kelvin-Helmholtz instability (KHI) and eventually converted to turbulence (e.g., Browning & Watkins, 1970). KHI in the atmosphere is characterized as the instability that occurs in a stratified fluid having strong vertical shear of horizontal winds. From the previous observational studies, it is shown that the KH billows in the mid-latitude are provided by a variety of atmospheric phenomena, such as cumulonimbus anvils (Petre & Verlinde, 2004), GWs (e.g., Fritts, 1979; Luce et al., 2008), air flows over mountainous terrain (Geerts et al., 2010; Mahalov et al., 2007; Medina & Houze, 2016), density currents associated with a sea breeze (Sha et al., 1991), tropospheric jets (Chilson et al., 1997; Klostermeyer & Rüster, 1980), cold fronts (Chapman & Browning, 1999; Geerts et al., 2006; Hardy et al., 1973; Samelson & Skyllingstad, 2016; Takayabu, 1992), and mid-latitude cyclones (Trier et al., 2020; Wakimoto et al., 1992). Nevertheless, there was no study of KH billows in the Antarctic based on direct observations. In addition, there are not many studies that refer to the excitation mechanisms of the KH billows observed by the remote sensing technique, not only in the polar regions but also in the mid-latitudes.

On the other hand, RWs have been examined by previous studies particularly for the stratosphere. However, studies of RWs in the mesosphere are limited because not many general circulation models cover the whole mesosphere, and observations of the mesosphere are difficult compared with those of the stratosphere. Garcia et al. (2005) reported that fast traveling planetary-scale waves are observed in the mesosphere and lower thermosphere (MLT) region by the observations of the Sounding of the Atmosphere using Broadband Emission Radiometry (SABER) instruments on board NASA's Thermosphere–Ionosphere–Mesosphere Energetics and Dynamics (TIMED) satellite. They showed quasi-2-day waves with zonal wavenumbers (s) of 2–4 are observed

during summer. Plumb (1983) also suggested that the quasi-2-day waves are generated from baroclinic instability of the summertime jet. Sato et al. (2018) revisited and examined the mechanisms of the dynamical instability from a PV viewpoint using simulation data over ~11 years from the Ground-to-Topside Model of Atmosphere and Ionosphere for Aeronomy (GAIA) (Jin et al., 2011). The model is nudged toward the JRA-25/JMA Climate Data Assimilation System (JCDAS) data (Onogi et al., 2007) for the altitude range from the surface to ~30km (12 hPa) in order to realistically simulate the quasi-biennial oscillation (QBO) in the equatorial stratosphere and planetary waves originating from the troposphere. The dynamical instability condition is characterized as the appearance of a PV maximum at middle latitudes. Poleward of it, the latitude gradient of PV becomes negative. It was shown that parameterized GW forcings, which mimic the forcings due to GWs originating from the troposphere in the GAIA, act to form the PV maximum in both the winter and summer mesospheres. Strong RWs propagating energy upward are generated slightly poleward of the PV maximum, which eliminate the PV maximum. SABER observations also reveal that waves with a zonal wavenumber (s) of 1 having a period of 4-5-day are dominant in the mesosphere, albeit only at certain times of the year. Lawrence & Randel (1996) pointed out that the 4-day wave appears in association with the instability of the polar night jet in the winter hemisphere. It is also shown that RWs with a 5-day wave period are observed by satellites and considered to be the gravest $s = 1$ normal mode RW of the Earth atmosphere having symmetric structure around the equator (Salby, 1981; Hirota et al., 1983; Hirooka & Hirota, 1985).

Yamazaki et al. (2020) reported that quasi-6-day oscillations in the equatorial electrojet having an $s = 1$ westward-moving wave-like structure were enhanced in the mesosphere during the SSW in the Southern Hemisphere in 2019. Several different excitation mechanisms have been proposed: Doppler-shift of 5-day normal mode waves (Wu et al., 1994), excitation from baroclinic and/or barotropic instability in the middle atmosphere (Lieberman et al., 2003; Liu et al., 2004; Meyer

& Forbes, 1997), and propagating from the troposphere to the mesopause (Talaat et al., 2002). Thus, the dynamical characteristics of waves with quasi-6-day wave periods observed in the mesosphere are not fully understood.

The Antarctic region is one of the essential regions for the middle atmosphere, because the start and end parts of the general material circulation are located in the stratosphere and mesosphere, as shown in Figure 1.1. It is important to elucidate the dynamics of the hierarchical structure in the Antarctic atmosphere, including GWs and RWs, which fundamentally contribute to understand the material circulation further. Due to the harsh environment, however, observations in the Antarctic were limited. In addition, high-resolution GCM simulations are still challenging for the MLT region.

1.3 The PANSY radar observation

The Program of the Antarctic Syowa (PANSY) radar was installed at Syowa Station (69.0°S, 39.6°E) in early 2011. This radar is the first Mesosphere-Stratosphere-Troposphere/Incoherent Scatter (MST/IS) radar in the Antarctic (Sato et al., 2014). The PANSY radar is a monostatic pulse VHF Doppler radar operated at 47 MHz in which an active phased array system consisting of 1,045 crossed-Yagi antennas is employed. Because MST radars receive scattering echoes from atmospheric turbulence, the PANSY radar is able to obtain wind measurements under any weather conditions. As the PANSY radar was successfully designed to save energy and can be operated with the total power consumption less than 70 kW, continuous operation over years is possible even in the Antarctic where the power supply is significantly limited.

A continuous full-system observation by the PANSY radar started on 1 October 2015. The observations provide vertical profiles of three-dimensional wind data, including vertical wind components. The time resolution is approximately 90 s, as an observation for the troposphere and

lower stratosphere and that for the mesosphere are alternately performed. The time interval for the one observation cycle is approximately 220 s. The range resolution (i.e., the vertical resolution of the vertical beam) is 150 m along its beam direction for the observations of the troposphere and lower stratosphere.

For the PANSY radar observations, five beams pointing to the vertical direction and to the north, east, south, and west at the same zenith angle (θ) of 10° are used. The accuracy of the line-of-sight velocity is about 0.1 m s^{-1}. The beam width of the PANSY radar observation is about 1.0 degree, corresponding to a horizontal resolution is about 26 m at 1.5 km, 150 m at 10 km, and 350 m at 20 km, for examples.

The data is processed in the digital signal processing unit for pulse decompression, coherent integration, and fast Fourier transform (FFT) operations to obtain the radio frequency spectra of back-scattering echo power. Line-of-sight velocities are estimated from the Doppler shift of the frequency spectra of echo scattered from the turbulences at each height using a least-square fit to a theoretically expected Gaussian function. Vertical wind velocities are directly estimated from the vertical beam, and zonal (meridional) wind components are obtained by combining a pair of line-of-sight velocities of the east (V_E) and west (V_{W}) beams (the north (V_{N}) and south (V_{S}) beams). It is a great advantage of MST radars that vertical winds can be directly observed. The radial velocities, V_{E} and V_{W} (V_{N} and V_{S}), are related to zonal (u) (meridional (v)) and vertical (w) components of winds as follows:

$$V_{\mathrm{E}} = u_{\mathrm{E}} \sin\theta + w_{\mathrm{E}} \cos\theta \,, \qquad V_{\mathrm{W}} = -u_{\mathrm{W}} \sin\theta + w_{W} \cos\theta \,, \tag{1-1}$$

where $u_{E(W)}$ and $w_{E(W)}$ are zonal and vertical component of wind in the target volume of the oblique beam pointing to the east (west). Assuming that the wind field is homogeneous between the beams at

each height (i.e., $u_{\mathrm{E}} = u_{\mathrm{W}} = u,\ w_{\mathrm{E}} = w_{\mathrm{W}} = w$), we can estimate u as follows.

$$u = \frac{V_E - V_W}{2\sin\theta}. \tag{1-2}$$

In addition, by assuming that the flux and variance fields are homogeneous (i.e., $\overline{u'_{\mathrm{E}}w'_{\mathrm{E}}} = \overline{u'_{\mathrm{W}}w'_{\mathrm{W}}} = \overline{u'w'}, \overline{u'^2_E} = \overline{u'^2_W} = \overline{u'^2},$ and $\overline{w'^2_E} = \overline{w'^2_W} = \overline{w'^2}$) the vertical flux of zonal momentum ($\overline{u'w'}$) is estimated using variances of radial wind fluctuations (Vincent & Reid, 1983):

$$\begin{aligned} \overline{V'^2_E} &= \overline{u'^2_E}\sin^2\theta + \overline{u'_{\mathrm{E}}w'_{\mathrm{E}}}\sin\theta\cos\theta + \overline{w'^2_{\mathrm{E}}}\cos^2\theta \\ \text{and } \overline{V'^2_{\mathrm{W}}} &= \overline{u'^2_{\mathrm{W}}}\sin^2\theta - \overline{u'_{\mathrm{W}}w'_{\mathrm{W}}}\sin\theta\cos\theta + \overline{w'^2_{\mathrm{W}}}\cos^2\theta\,. \end{aligned} \tag{1-3}$$

The $\overline{u'w'}$ is obtained from the difference of the variances of radial wind fluctuations from the east and west beams ($\overline{V'^2_{\mathrm{E}}}$ and $\overline{V'^2_{\mathrm{W}}}$):

$$\overline{u'w'} = \frac{\overline{V'^2_{\mathrm{E}}} - \overline{V'^2_{\mathrm{W}}}}{2\sin 2\theta}, \tag{1-4}$$

where the prime and overline represent GW components and a time average, respectively. The meridional component ($\overline{v'w'}$) can be calculated in the same way. It is worth noting that the assumption used for estimating the momentum fluxes is less strict than that for the horizontal winds.

Continuous observation data with a fine time resolution over ~26 hours allows us to analyze almost the entire frequency range of GWs. The frequency of GWs ranges from the inertial frequency (f) of $\sim 2\pi/(13\ \mathrm{h})$ at Syowa Station to the buoyancy frequency (N) of $\sim 2\pi/(10\ \mathrm{min})$ in the troposphere and of $\sim 2\pi/(5\ \mathrm{min})$ in the stratosphere, when the Doppler shift by the background wind is negligible. The buoyancy frequency is also called the Brunt-Väisälä frequency.

Using observation data from the PANSY radar over a year from October 2015 to September 2016, Minamihara et al. (2018) showed that frequency power spectra of u' and v' have an isolated peak near the inertial period at Syowa Station ($2\pi/f$, ~13 h) This maximum is quite remarkable in

the lower stratosphere in the height region of $z > 11$ km. They also showed statistical characteristics of the GWs having near-inertial frequencies. Throughout the year, GWs with upward group velocities are dominant in the middle and lower troposphere. On the other hand, a considerable proportion of the GWs propagates energy downward in the upper troposphere during all seasons and above a height of 15 km in winter. The presence of the GWs propagating energy downward in the stratosphere is a characteristic feature in the Antarctic (Yoshiki & Sato, 2000). These results suggest that plausible candidates of the GW sources over Syowa Station are topography (Minamihara et al., 2016), the tropospheric jet, and the polar night jet.

Furthermore, Minamihara et al. (2020) examined the intermittency of GWs having near-inertial frequencies observed by the PANSY radar in the troposphere and lower stratosphere. They showed that the intermittency is large in the troposphere and small in the lower stratosphere. They suggested that the generation and the partial reflection of GWs play an important role in determining the vertical profile of GW intermittency. It was also shown that the intermittency is large even in the stratosphere a few times a year when quite strong tropospheric disturbances penetrating the stratosphere are observed.

Yoshiki & Sato (2000) examined GWs in the Antarctic lower stratosphere using operational radiosonde observation data taken at 21 stations located at high latitudes of the Southern Hemisphere. They showed that the GWs over Syowa Station have typical characteristics as those in the coastal region of the Antarctic continent. In the Antarctic, the potential and kinetic energies of GWs vary annually and are maximized in spring, and GW energy in the lower stratosphere showed a high correlation with the stratospheric mean wind speed. Furthermore, they indicated that the GW energy maximum in spring corresponds well to the enhancement of N^2.

Radiosondes and satellites are also used to observe GWs. Satellite observations allow us to estimate the global distribution of GW properties and momentum fluxes mainly in the stratosphere.

From temperature data obtained by the Cryogenic Infrared Spectrometers and Telescopes for the Atmosphere (CRISTA), localized and intense wave packets emitted from the topography are often observed (Ern et al., 2004; Preusse et al., 2002). Nevertheless, it is worth noting that satellite instruments cannot resolve the whole wavelength range of all the propagating GWs in the middle atmosphere (observational filter) (Alexander, 1998). For example, nadir sounding has an advantage in observing GWs with large horizontal wavenumbers, while they cannot adequately capture GWs having large vertical wavenumbers. Limb sounding, on the other hand, can observe GWs with large vertical wavenumbers, whereas they are not able to capture GWs with large horizontal wavenumbers (Preusse et al., 2008).

Super-pressure balloon observations performed such as Vorcore (Hertzog et al., 2007) and Concordiasi (Rabier et al., 2010) campaigns also provide unique data for GWs in the lower stratosphere over Antarctica and the Southern Ocean. The data from the super-pressure balloon observations were limited to the duration and trajectory of the flight. However, the observation can detect GW frequencies relative to the mean wind, namely, intrinsic frequencies. This means that we can make analysis free from the Doppler shift by the mean wind. Using these data, Hertzog et al. (2012) analyzed orographic and non-orographic waves separately. They reported significantly high intermittency above the Antarctica and the Southern Ocean. They also indicated that the magnitude of horizontal pseudo-momentum flux was about 100 mPa.

Radiosonde observations provide horizontal wind and temperature data with high resolution in the vertical. Yoshiki et al. (2004) used radiosonde data at Syowa Station and indicated that the GW energy is enhanced when the edge of the polar vortex approaches Syowa Station and the polar vortex tends to break. Sato & Yoshiki (2008) performed three-hourly radiosonde observation campaigns over 10 days in each month of March, June, October, and December 2002 at Syowa Station. They examined the characteristics of the inertia GWs in the lower stratosphere and indicated that

some of these GWs were likely emitted upward and downward through a spontaneous adjustment around an imbalance of the polar night jet located at a slightly lower latitude than Syowa Station.

1.4 General circulation models permitting gravity waves

Most GCMs used for weather prediction and climate projection include GW parameterizations because GWs are usually sub-grid-scale phenomena in the models. However, a recent development in supercomputer technology allows us to simulate a significant part of GWs explicitly in high-resolution GCMs (e.g., Hamilton et al., 1999; Sato et al., 1999; Shibuya et al., 2017; Watanabe et al., 2008; Watanabe & Miyahara, 2009). Although the full spectral range of GWs is not fully resolved, it was indicated that large-scale wind and temperature fields could be realistically simulated by such high-resolution GCMs without GW parameterizations. This fact suggests that behaviors of the resolved GWs are simulated well in terms of propagation and dissipation.

A few GW-permitting GCMs were achieved to raise the model top higher up to the MLT region. A GW-permitting GCM of the KANTO project (hereafter called the KANTO model) was developed for studying middle atmosphere dynamics including the role of GWs in the global atmosphere (Watanabe et al., 2008). The KANTO model has a spatial resolution of a triangular spectral truncation at a total horizontal wavenumber of 213 (T213) and 256 vertical levels (L256) extending from the surface to a height of 85 km with a uniform vertical spacing of 300 m. The minimum resolvable horizontal wavelength of the model is 180 km. A simulation was performed over three model years and output averaged over 1 hour were saved. The outputs are used for the dynamical analysis as a surrogate of the real atmosphere. All GWs are spontaneously generated by convection, topography, instability, and adjustment processes in the model. The model could reproduce realistic zonal mean zonal wind and temperature in the middle atmosphere. This model was only model in the

world that could simulate the quasi-biennial oscillation (QBO)-like phenomenon in the equatorial stratosphere without using GW parameterizations, although the oscillation period was short compared with the real atmosphere. Watanabe et al. (2008) examined the wave forcing due to planetary waves and GWs. They showed that the GW forcing causes deceleration of the wintertime polar night jet and the summertime easterly jet in the mesosphere. In contrast, extratropical planetary waves primarily cause deceleration of the polar night jet below a height of approximately 60 km. They also indicated that the meridional distribution and propagation of small-scale GWs affect the shape of the upper part of mesospheric jets. Sato et al. (2009) examined a global view of GW sources and propagation in the mesosphere using the KANTO model. They showed that GWs propagating from the subtropics in summer and those from the middle to high latitudes in winter tend to focus on the mesospheric jets of respective hemisphere, causing effective deceleration of the jet. By analyzing the horizontal distribution of the momentum fluxes, they also indicated that the dominant sources of GWs are steep mountains, and jet-front system in winter, and vigorous monsoon convection in summer. Watanabe et al. (2009) investigated the eastward-propagating 4-day wave with s = 1–4 in the Antarctic winter mesosphere using the KANTO model data. They showed that the simulated 4-day waves develop due to the baroclinic and barotropic instability in the mesosphere originally caused by GW forcing. Tomikawa et al. (2012) examined recovery formation and processes of a major SSW including appearance of an elevated stratopause and reformation of the strong polar-night jet using the KANTO model simulation. The major SSW spontaneously occurred in the KANTO model bears a strong resemblance to the real major SSWs in January 2006 and January 2009. They showed that there are two stages in the recovery phase of the SSW. In the first stage during about five days just after the SSW, a large positive wave forcing associated with the growth of planetary waves contributes to a quick recovery of eastward wind above 2 hPa (about 42 km). In the second stage over subsequent three weeks, a prolonged westward wind in the lower stratosphere blocked the upward propagation

of GWs having westward intrinsic phase velocities by critical level filtering. It reduces the deceleration of eastward wind in the upper mesosphere and raises the breaking height of GWs. The polar stratopause is maintained by meridional circulation mainly driven by GW forcings. Thus, the polar stratopause is reformed at an elevated height (~ 75 km) compared to that before the SSW (55–65 km).

Kühlungsborn Mechanistic Circulation Model (KMCM) (Becker, 2009) has a spatial resolution of T120, corresponding to a minimum horizontal wavelength of 350 km. There are 190 full-hybrid levels in the vertical grids from 990 hPa to 2×10^{-5} hPa with grids spacing of ~ 600 m between the boundary layer and 3×10^{-4} hPa (~ 105 km). There is no parameterization of GWs. Hoffmann et al. (2010) investigated the seasonal variation of the GW activity in the MLT region using wind observations by the meteor radars and a numerical simulation by the KMCM. The observed strong easterly winds had a peak around $z = 75$ km in summer. This easterly jet strengthened abruptly from spring to summer. The KMCM also reproduced characteristics of the annual cycle of the zonal winds and the strongest GW energy during winter and summer. A new version of the KMCM with T240L190 represents primary GWs generated by fronts and nonlinear dynamics of RWs in the troposphere (Plougonven & Zhang, 2014), as well as by topography. They reasonably simulated the medium-scale orographic GWs in the middle atmosphere from the most prominent hotspots. In addition, Secondary GWs excited by a body force due to orographic GWs during winter were also simulated. Yasui et al. (2018) and Yasui & Sato (2021) also suggested that the forcing by GWs originating from the lower atmosphere causes the shear instabilities that generate secondary GWs as well as the barotropic/baroclinic in the mesosphere using simulation data from the GAIA model.

Liu et al. (2014) examined simulation results from the Whole Atmosphere Community Climate Model version 5 (WACCM5) extending from the surface to $z =$ ~145 km with a horizontal resolution of ~0.25° and a vertical resolution of 0.1 scale height. They examined the resolved GWs,

including their horizontal and vertical structures, spectral structures, and the wave forcing on the mean flow. It was shown that concentric GWs spreading almost a third of the globe in the MLT region were seen in the low to middle latitudes. The GWs were likely excited by deep convection. In the middle to high latitudes in the winter hemisphere, they also indicated the strong wave perturbations above the stratosphere, probably excited by the spontaneous adjustment of the jet. The distribution of the wave activities in the WACCM5 was in good agreement with those deduced from the Sounding of the SABER observations.

Shibuya et al. (2017) examined the dynamical characteristics and excitation mechanism of GWs in the mesosphere observed by the PANSY radar using the Nonhydrostatic Icosahedral Atmospheric Model (NICAM) (Satoh et al., 2008; 2014) simulations. The NICAM in this study had the vertical grid spacing of ∼400m (L217) and the horizontal icosahedral grids with g-level 7 (corresponding to $\Delta x \sim 56$ km). They showed that quasi-12 h disturbances with horizontal wavelengths longer than 1400 km are dominant in the mesosphere over Syowa Station by the NICAM simulation. The parameters of the simulated waves are consistent with the inertia GW observed by the PANSY radar. They also indicated that the inertia GWs are likely generated by the spontaneous radiation mechanism of the mid-latitude tropospheric jet and polar night jet. Shibuya & Sato (2019) also showed that the power spectrum of the wind fluctuations at $z = 70$ km has an isolated and broad peak at frequencies slightly lower than the inertial frequency at each latitude of 30°S–75°S in consecutive numerical simulations by NICAM. It is also shown that the isolated peak is composed of GWs having horizontal wavelengths of more than 1000 km. They noted that the existence of the isolated peak in high latitudes is likely explained by the poleward propagation of quasi-inertia GWs and by the accumulation of wave energies near the inertial frequency at each latitude.

Watanabe & Miyahara (2009) examined the interaction of GWs and the migrating diurnal tide in two simulations for 15-day time periods in the perpetual equinoctial and solstice by the

Japanese Atmospheric General circulation model for Upper Atmosphere Research (JAGUAR) high-resolution GCM. They simulated the amplitudes of the migrating diurnal tide successfully during both seasons. They showed that the tidal winds affected the altitudes of GW dissipation associated with GW forcing. Watanabe et al. (2015) also showed that GW momentum fluxes are not heavily dependent on model vertical spacing in the middle atmosphere for $\Delta z < 400$ m.

As Shibuya & Sato (2019) reported that quasi-inertia GWs with wavelengths of more than 1000 km are dominant in the mesosphere, a major part of GWs inherently distributed over a wide horizontal wavelength range can be resolved in the GW-permitting models even in the mesosphere. Furthermore, Sato et al. (2017) examined GW momentum fluxes in the summer mesosphere using continuous mesospheric wind observation over 50 days by the PANSY radar. They showed that GWs with long periods of several hours to a day are dominant in the summer mesosphere. In the stratosphere, Minamihara et al. (2018) showed that dominant nearly-inertia GWs have horizontal wavelengths of 200–300 km based on the 1-year continuous observations by the PANSY radar. Ern et al. (2018) also showed dominant GWs in the middle atmosphere on average have horizontal wavelengths greater than 1,000 km and vertical wavelengths longer than 10 km by the satellite observation data. However, it should be emphasized that the observational filter problem remains.

In this thesis, we performed numerical simulations using GW-permitting GCMs to elucidate the dynamical structure of GWs captured by the PANSY radar and radiosondes. These models have sufficient resolution to resolve the GWs that are considered to be dominant in the mesosphere. The vertical resolution also satisfies the requirement to represent the momentum fluxes of GWs (Watanabe et al., 2015). In Chapter 2, we carried out the NICAM simulations to examine the spatial structure of GWs in the troposphere and lower stratosphere and a cyclone approaching Syowa Station. They likely caused the KH instability captured by the PANSY radar. In Chapter 3, we conducted the simulations using the JAGUAR to investigate the spatial structure of the characteristic wave-like structures

observed above Syowa Station during the SSW in the Southern Hemisphere in September 2019. The JAGUAR simulation data are also used to analyze the spatial distributions and time variation of RWs and GWs from the troposphere to the MLT region during the SSW event in the Southern Hemisphere in September 2019.

1.5 Overview of this thesis

Various atmospheric disturbances over a wide-scale range, from atmospheric turbulence to the polar vortex, constitute the atmospheric hierarchical structure (Figure 1.2). So far, only a part of the hierarchical structure, such as the interplay of GWs and RWs (Sato and Nomoto, 2015), has been shown, and other dynamical relations among phenomena with different scales remain poorly understood. In particular, the understanding of the hierarchical structure in the Antarctic atmosphere was limited due to the shortage of observations. In this thesis, we will elucidate the dynamical structure of each atmospheric phenomenon and its role in the hierarchical structure using the observations and numerical model simulations. In particular, we will focus on the role and relations including GWs captured by the PANSY radar and simulated by high-resolution GCMs.

The author participated in the 60th Japanese Antarctic Research Expedition from October 2018 to March 2020 and carried out two observational campaigns at Syowa Station in the Antarctic. One is a synchronized observation with the PANSY radar and radiosondes for 20 days focusing on the atmospheric turbulence in the troposphere and lower stratosphere. In Chapter 2, we will focus on the hierarchical structure for relatively small scales, from atmospheric turbulences to cyclones, including GWs (Figure 1.2). Specifically, we will examine how KH billows in the Antarctic region are excited, and what atmospheric phenomena in the Antarctic excite KH billows. The other is a simultaneous observation by the PANSY radar and radiosondes focusing on the wave-like

disturbances in the lower stratosphere associated with the SSW in August and September 2019. In Chapter 3, we will address the hierarchical structure for relatively large scales from GWs to the polar vortex during the SSW event (Figure 1.2). In particular, it is not fully understood how the distribution of GWs from the troposphere to the lower thermosphere temporally varied during the SSW in the Southern Hemisphere in 2019, and how the quasi-6-day waves in the mesosphere were excited.

This thesis is organized as follows. Chapter 2 shows the study on Kelvin-Helmholtz billows detected by the PANSY radar using a frequency domain interferometry technique. Chapter 3 shows the study on the dynamical characteristic of GWs and RWs during the SSW in the southern hemisphere in 2019. Summary of this thesis and concluding remarks are given in Chapter 4.

Chapter 2. Kelvin-Helmholtz billows detected by the PANSY radar using a frequency domain interferometry (FII) technique

本章の内容は、5 年以内に学術誌等に刊行予定のため、非公開とする。

Chapter 3. Dynamical analysis of gravity waves and Rossby waves in the neutral atmosphere during the stratospheric sudden warming in the Southern Hemisphere in 2019

本章の内容は、5 年以内に学術誌等に刊行予定のため、非公開とする。

Chapter 4. Summary and conclusion remarks

This study analyzed the relations among atmospheric phenomena included in the in the hierarchical structure of the Antarctic atmosphere. We used the PANSY radar and radiosonde observations with high accuracy and high resolution, and the numerical simulations by the GW-permitting GCMs. In particular, we focused on the KH billows, GWs, and the polar vortex during the SSW-SH 2019 seen in the observational campaigns performed at Syowa Station in 2019.

In Chapter 2, we examined on the relations among relatively small-scale disturbances, from KH billows to synoptic-scale waves (Figure 4.1). During 14–24 March and 2–12 August 2019, the observational campaigns targeting atmospheric turbulence in the troposphere and lower-atmosphere were performed with the PANSY radar and radiosondes. A total of 73 S-shaped structures, which are characteristic of KH billows, were detected by the PANSY radar with the FII technique during the campaigns. Numerical simulations using NICAM were also performed in order to investigate the spatial structure of the GWs and cyclone related to the excitation of the observed KH billows.

First, a detailed study for two representative cases out of all observed KH billows was performed. The first case is the KH billows with the longest duration (Case A). The horizontal wind disturbance with a vertical wavelength of ~1.5 km was dominant in the height region where the KH billow of Case A was observed. This horizontal wind disturbance was amplified below the weak wind layer. Assuming that this horizontal wind disturbance was an inertia GW, we performed hodograph analysis on the horizontal disturbance. It was shown that the wave had an upward group velocity, a horizontal wavelength of ~145 km, a vertical wavelength of ~1.6 km, and a ground-based horizontal phase velocity of ~2.3 m s^{-1}. These features were consistent with the dynamical characteristics of an orographic GW. According to the NICAM simulations, a cyclone was located about 500 km to the north-northwest of Syowa Station during Case A. Around Syowa Station, the north-easterly wind of ~25 m s^{-1} blew up the coast slope of the Antarctic continent. The wave-like structure over Syowa

Station had a phase line tilted upwind with altitude. These results strongly support that the KH billow in Case A was caused by the strong vertical shear associated with the orographic GW.

The second case is the KH billow having the deepest vertical structure (Case B). In the height region where the KH billow of Case B was observed, wave-like structures were not found over Syowa Station unlike Case A, but there was strong vertical shear in the bottom of the northerly jet in the upper troposphere. The upper tropospheric jet was associated with a cyclone located about 500 km to the northwest of Syowa Station. This cyclone was most developed around 55°S about two days before Case B. The baroclinic instability likely developed this cyclone and formed peaks of meridional wind disturbances around the surface and the tropopause. It was also shown that the cyclone entrained and stretched high-temperature air mass from low latitudes. This air mass with high temperature was cut off from low latitudes and advected over Syowa Station. The localized thermal wind balance associated with this air mass likely strengthened the upper tropospheric jet over Syowa Station. These results indicate that the KH billow in Case B was caused by the strong vertical shear associated with the enhanced upper-tropospheric jet.

This study revealed that there are at least two kinds of generation mechanisms of KHI in the Antarctic region: orographic GWs and a tropospheric jet localized in the upper troposphere associated with a cyclone. It is known that orographic GWs are dominant in the troposphere and lower stratosphere above the Antarctic coastal region with steep topography. In addition, it was reported that cyclones approaching the Antarctic continent have a shrunken meridional scale and an enhanced westerly jet associated with a strong meridional gradient of potential vorticity due to radiative cooling on the slope of the Antarctic continent (M. Mizukoshi's master thesis). Thus, these two excitation mechanisms of KH billows well reflect the characteristics of the Antarctic coastal region: the steep coastal topography and the well-developed synoptic-scale cyclones.

Comparisons with the most unstable modes expected from a two-dimensional linear

stability theory were made for Case A and Case B. The expected most unstable modes were generally consistent with the dynamical characteristics of the observed KH billows, although the horizontal wavelength and the depth expected from the theory were slightly shorter than those of the observed billows. In addition, a statistical analysis of all 73 captured KH billows was performed. This study also shows the dynamical characteristics of KH billows in the Antarctic region statistically for the first time. The mean and probability density function of the horizontal wavelength, thickness, and aspect ratio of all 73 observed KH billows waves are almost the same as those estimated by the mid-latitude observations. Furthermore, there was no distinct difference between the statistic values in March and August. On the other hand, the magnitude of vertical shear of the background wind is about 60 % of that estimated at the mid-latitude. Moreover, the wave period of the KH billows is about twice as long as that of the KH billows observed at the mid-latitude. These differences likely reflect the fact that the tropospheric jet in the Antarctic is not as strong as the jet over Japan.

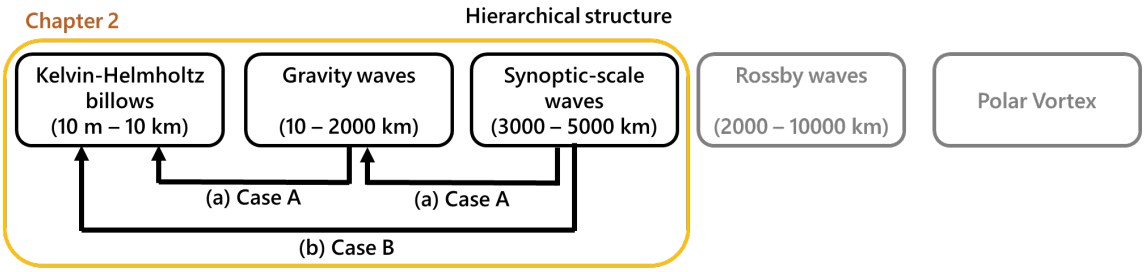

Figure 4.1: A schematic illustration of the relations in the hierarchical structure shown in Chapter 2. (a) Strong winds around the surface associated with a synoptic-scale cyclone generate orographic GWs. The continuous injection of GW energy by the strong winds maintains the shear instability for a long time (Case A). (b) Shear instability was formed by the upper tropospheric jet associated with a synoptic-scale cyclone. This shear instability is vertically thicker than that associated with orographic GWs, and the generated KH billows have a deeper structure (Case B).

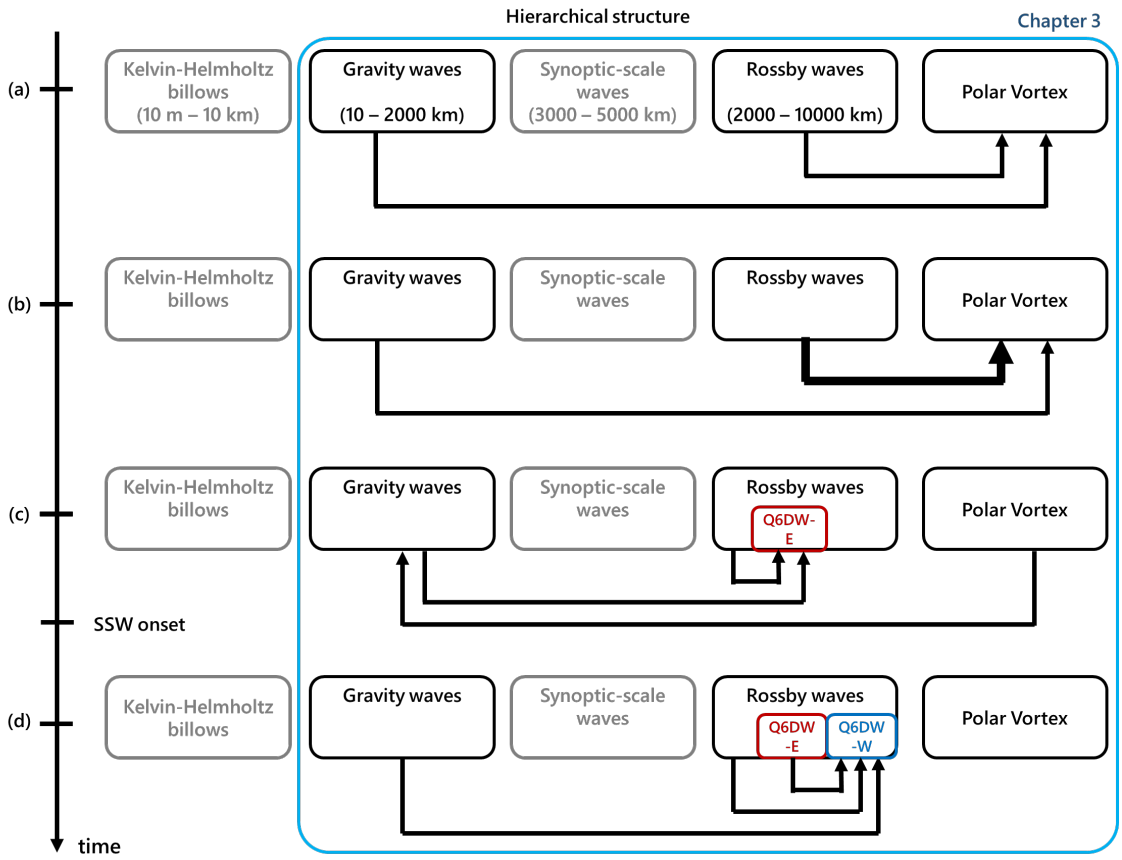

Figure 4.2: A schematic illustration of the relations in the hierarchical structure shown in Chapter 3. (a) Ordinary conditions before the SSW. The shape and strength of the polar vortex, which is formed by latitudinal difference of radiative heating, is maintained by RWs and GWs propagating from the troposphere. (b) Strong RWs propagate into the stratosphere, break, and cause the SSW. During the SSW, the polar vortex shifts to lower latitudes and the upper part of the polar vortex disappears. (c) Weakening and shift of the polar vortex modify the distribution of GWs. Negative RW and GW forcing in the mesosphere contribute to the excitation of the Q6DW-E. (d) GWs, RWs propagating from the mid- and high-latitude troposphere, and the Q6DW-E provide barotropic/baroclinic instability in which the Q6DW-W is excited.

In Chapter 3, we investigated the relations among relatively large-scale atmospheric phenomena from GWs to the polar vortex (Figure 4.2). In particular, we focused on the dynamical characteristics of GWs and RWs during the SSW-SH 2019. Simultaneous observations with the PANSY radar and radiosondes were performed in order to examine the wind and temperature disturbances in the lower stratosphere during the SSW-SH 2019. In addition, numerical simulations using the high-resolution JAGUAR (T639L340) from the surface to the MLT region were also made to investigate the spatial distribution and momentum budget GWs and RWs, especially Q6DWs, during the SSW-SH 2019.

First, we confirmed that the high-resolution JAGUAR reproduces the appearance and distribution of wave-like structures in the lower stratosphere, which is considered to be GWs, observed by the PANSY radar and radiosondes. On the other hand, it was suggested that the magnitude of GW momentum fluxes in the high-resolution JAGUAR simulations is about one-fifth of that in the real atmosphere. It may be due to the fact that GWs with large horizontal wavenumbers and/or high frequencies are not sufficiently reproduced in the high-resolution JAGUAR simulations.

We also examined the wave forcing associated with RWs and GWs and residual circulations (Section 3.3). The RW forcing in the height region of z = 30-60 km and at 50°S-70°S are dominant before 7 September. The negative RW forcing weakened the polar vortex and eventually led to the SSW-SH 2019 (Figure 4.2b).

Next, we examine the dynamical structures of the GWs over Syowa Station using the high-resolution JAGUAR simulations. It was found that GWs with large amplitude were observed in the stratosphere when the polar vortex shifted to the Western Hemisphere and the edge of the vortex approached Syowa Station. In addition, the V-shaped increase in temperature observed in the lower stratosphere corresponded to the region with high temperature in the poleward side of the polar vortex displaced to the Western Hemisphere. For the distribution of GWs, we found that the largely negative

GW momentum fluxes ($\overline{u'w'}$) in the stratosphere were observed over the Andean Mountains and the Antarctic Peninsula before 7 September (the SSW onset) and above and leeward of the Ross Sea after the onset. On the other hand, above $z = 75$ km, largely negative $\overline{u'w'}$ and GW energy were observed to the south of 40°S before 3 September. During 3–10 September when the polar vortex became obscure, positive $\overline{u'w'}$ was seen around 60°S. When the polar vortex reappeared after 10 September, negative $\overline{u'w'}$ was observed to the south of 40°S again, although its magnitude was smaller than that before 3 September (Figure 4.2c).

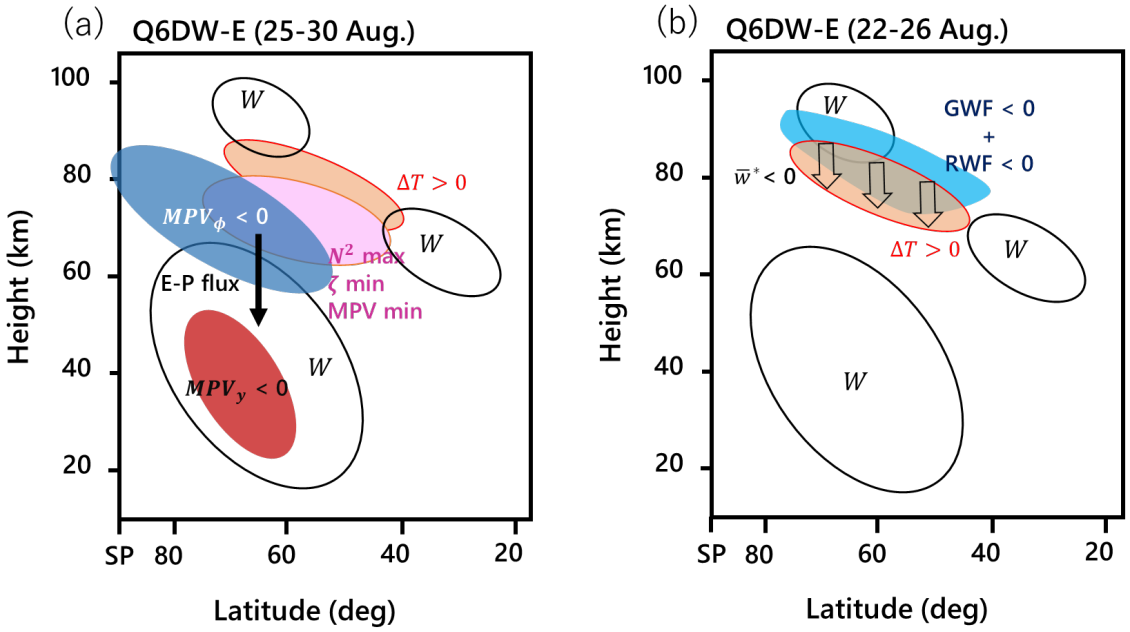

Figure 4.3: Schematic illustrations of excitation mechanisms of Q6DW-E on (a) 25–30 August and (b) 22–26 August.

We also investigated the spatial structures of Q6DW using the JAGUAR-DAS analysis data and high-resolution JAGUAR simulations. The peaks of the frequency spectra are seen in both the westward and eastward phase velocity components with a period of about six days. The Q6DW-Es were dominant to the south of 40°S before 10 September, and Q6DW-Ws were dominant in both

795 hemispheres centered at 40° latitude after 10 September. Moreover, the Q6DW-E had the phase of GPH disturbances tilted eastward with altitude above $z = 50$ km, and the Q6DW-W had the phase of GPH disturbances tilted westward with altitude above $z = 60$ km. These baroclinic structures are different from the normal mode 5-day Rossby wave which is an external wave having a barotropic structure.

800 Next, we investigated the excitation mechanisms of Q6DW-E and Q6DW-W. It was suggested that the Q6DW-E is an unstable wave due to the baroclinic-instability characterized as a pair of the negative MPV meridional gradient ($\mathrm{d}MPV/\mathrm{d}y < 0$) in the mesosphere in the high latitude and the positive MPV gradient ($\mathrm{d}MPV/\mathrm{d}y > 0$) in the stratosphere (Figure 4.3a). This inference is supported by the fact that the region with $\mathrm{d}MPV/\mathrm{d}y < 0$ in the mesosphere disappear when the
805 Q6DW-E was no longer observed. The negative and positive $\mathrm{d}MPV/\mathrm{d}y$ were associated with the minimum and maximum of MPV located slightly equatorward of them. The MPV minimum in the mesosphere was maintained by the N^2 maximum and the ζ minimum (Figure 4.3a). The ζ minimum was corresponded to the westerly jet tilted poleward with height in the mesosphere. In the formation of the N^2 maximum, the negative RWs and GWs forcing extending from $z = 90$ km at 80°S to $z =$
810 80 km at 40°S played an important role (Figure 4.2c). This downward residual circulation driven by the negative forcings provided positive temperature anomaly through the adiabatic heating in the same region (Figure 4.3b), which leads to the N^2 maximum in the lower part of the region. Sato et al. (2018) reported that the region with $\mathrm{d}MPV/\mathrm{d}y < 0$ in the mesosphere is also found in the climatology.

815 On the other hand, Q6DW-W is likely to be an internal RW generated from barotropic/baroclinic instability in the upper stratosphere over 60°S–80°S. This dynamic instability was associated with the MPV local minimum corresponding to the broad N^2 maximum at 40°S–70°S and $z = 40$–50 km (Figure 4.4a). We also indicated that the N^2 maximum was caused by a downward

residual flow spreading from $z =$ 50 km at 80°S to $z = 60$ km at 40°S on 7–12 September (Figure 4.4b). This downward residual circulation was partly driven by the positive RW forcing associated with the Q6DW-E spreading from $z = 50$–80 km at 80°S to $z = 70$ km at 40°S and negative wave forcing due to Q6DW-E and the convergence of RW propagating from the troposphere from $z < 40$ km at 80°S to $z < 60$ km at 40°S. In addition, the positive GW forcing in the region from $z = 50$-80 km at 80°S to $z = 70$ km at 40°S, where the polar vortex displaced with the SSW, and the negative GW forcing in the region from $z < 40$ km at 80°S to $z < 60$ km at 40°S, where the polar night jet still existed, had almost the same magnitude as the RW forcing and played a significant role in the formation of the circulation (Figure 4.2d). The excitation mechanisms of the Q6DW-E and Q6DW-W were consistent with the fact that Q6DW-E appears every winter in both hemispheres in the high latitudes and Q6DW-W does not appear obviously except in September 2019 when an SSW occurred in the Southern Hemisphere. The positive GW forcing in the mesosphere associated with the shifted polar vortex during the SSW is a unique feature in September 2019. On the other hand, Q6DW-W dominance in both hemispheres was observed only in September 2019 and nor clearly found in February 2018 or January 2019, when the SSW occurred in the Northern Hemisphere (Figure 3.24a). It suggests that other mechanisms other than the occurrence of the SSW can also contribute to the generation of the Q6DW-W.

In addition, it was shown that the E-P fluxes associated with the Q6DW-W crossed the equator at $z = 85$–100 km on 10–15 September. This result suggested that the Q6DW-W originated from the Southern Hemisphere and spread to the Northern Hemisphere. Furthermore, the Q6DW-W propagating from the Southern Hemisphere may cause the barotropic and/or baroclinic instability in the region of $\mathrm{d}MPV/\mathrm{d}y < 0$ in the Northern Hemisphere (Figure 3.33), and internal RWs generated in the Northern Hemisphere as well as the Southern Hemisphere. However, this mechanism cannot explain the phase coincidence of Q6DW-W between the Northern and Southern Hemispheres. It is

also possible that Q6DW-W excited in the Southern Hemisphere led to a situation where Q6DW-W is generated from the region of $\mathrm{d}MPV/\mathrm{d}y < 0$ in the Northern Hemisphere through the normal mode 5-day waves with a coordinate phase structure in both hemispheres, which is similar to the Q6DW-W.

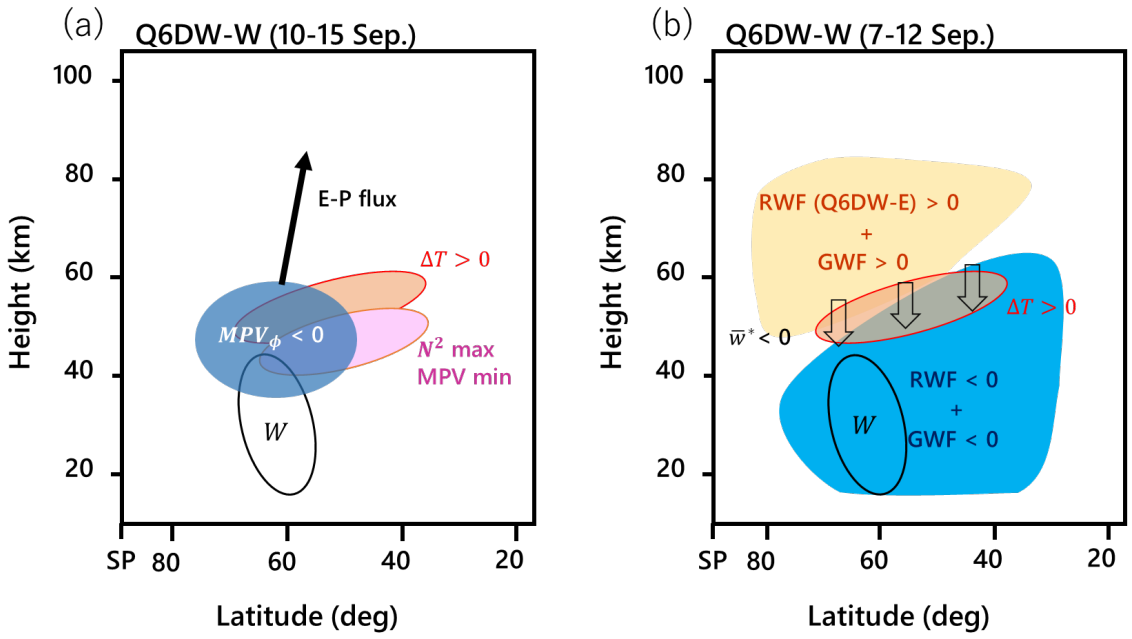

Figure 4.4: Schematic illustrations of excitation mechanisms of Q6DW-W (a) on 10–15 September and (b) 7–12 September.

Focusing on the relations within the hierarchical structure, we suggested that the orographic GWs and cyclones having the enhanced upper-tropospheric jets excite KH billows in the Antarctic coastal region in Chapter 2. They are characteristic phenomena in the Antarctic coastal region. In Chapter 3, we confirmed that RW and GW forcings weakened the polar vortex and eventually led to the SSW-SH 2019. We also showed how the GW distribution varies with the shift of the polar vortex during the SSW-SH 2019. For Q6DWs, we indicated that the mesospheric RW and GW forcings contribute to the excitation of Q6DW-E. We also suggested that the Q6DW-E forcing and the positive GW forcing associated with the

shifted polar vortex likely contributed to the excitation of internal RWs, namely Q6DW-W, from the barotropic and/or baroclinic instability (Figure 4.2d). However, the relations among atmospheric phenomena with different temporal and spatial scales shown in this study are only a part of the hierarchical structure in the Antarctic atmosphere. More studies using both high resolution observations and numerical simulations utilizing GW-permitting GCMs are necessary to understand the hierarchical structure further. In particular, an accumulation of case studies is essential for elucidating where there are other new excitation mechanisms of KH billows and for estimate of statistical significance for the mean values and probability density function of KH billows characteristics. The PANSY radar observation provides vertical profiles of turbulent kinetic energy dissipation rate, although they were not used for the analysis. This information must be valuable to verify the temporal and spatial distribution of the parameters describing the turbulence in the GCMs such as vertical diffusivity for the development of turbulence schemes in the free atmosphere.

It is also interesting to confirm the robustness of the excitation mechanism of Q6DW shown in this study. The examination of the interannual variation of Q6DW is necessary in terms of the Q6DW-E forcing and GW forcing, which is a key for the excitation mechanism of Q6DW-W. The investigation what determines the time lag between the appearance of the barotropic/baroclinic instability and the onset of Q6DW-W dominance is also future work.

Finally, the PANSY radar started meteor wind observations from the end of February 2021. The meteor wind observation enables us to continuously observe three-dimensional wind in the mesosphere with lower temporal and range resolutions compared with the standard observations. In the standard observation, three-dimensional winds are sparse in the weak solar radiation condition in winter. The continuous observational data of the three-dimensional mesospheric wind will contribute to further understanding of the hierarchical structure especially in the mesosphere. Additionally, it will enable the validation of simulations in the mesosphere and contribute to the development of high-

880 top GCMs permitting GWs.

Acknowledgements

I would like to express my sincere gratitude to my supervisor Prof. Kaoru Sato. I also thank Profs. Masahiro Watanabe, Yu Kosaka, Yukio Masumoto, and Keita Iga for their many helpful comments and discussions. I am grateful to Profs. Masaki Tsutsumi at National Institute of Polar Research (NIPR) for useful comments, Profs. Hiroshi Niino at Atmosphere and Ocean Research Institute for helpful advice, and Dr. Shingo Watanabe at Japan Agency for Marine-Earth Science and Technology for the numerical simulations using the JAGUAR. Special thanks are given to colleagues and former members in the atmospheric dynamics laboratory: Dr. Masashi Kohma, Dr. Yukari Sumi, Dr. Maria Mihalikova, Mr. Masahiro Nomoto, Dr. Yuki Yasuda, Dr. Ryosuke Shibuya, Dr. Arata Amemiya, Dr. Soichiro Hirano, Mr. Yuki Hayashi, Dr. Ryosuke Yasui, Mr. Dai Koshin, Mr. Shun Nakajima, Mr. Yuki Matsushita, Ms. Haruka Okui, Mr. Masatoshi Mizukoshi, and Mr. Kenta Aoishi. Finally, I thank all the members of the 60th Japanese Antarctic Research Expedition (JARE60) for their enormous support of the observation at Syowa Station in the Antarctic.

This study was supported by JST CREST grant JPMJCR1663 and JSPS KAKENHI grants 201703536. PANSY is a multi-institutional project with core members from The University of Tokyo, the National Institute of Polar Research, and the Kyoto University. The PANSY radar and radiosonde measurements at Syowa Station are operated by the JARE. The PANSY radar observational data are available at the project website, http://pansy.eps.s.u-tokyo.ac.jp. Radiosonde observation data at Syowa Station were provided by the Japan Meteorological Agency. Numerical simulations by the NICAM were run on the NIPR supercomputer and the computational resource of Fujitsu PRIMERGY CX600M1/CX1640M1 (Oakforest-PACS) was awarded by "Large-scale HPC Challenge" Project, Joint Center for Advanced High Performance Computing (JCAHPC). The hindcasts by the JAGUAR were performed using the Earth Simulator at the JAMSTEC. All figures except citations were created

905 using the Dennou Club Library (DCL).

References

Alexander, M. J. (1998). Interpretations of observed climatological patterns in stratospheric gravity wave variance. *Journal of Geophysical Research: Atmospheres*, *103*(D8), 8627–8640. https://doi.org/10.1029/97JD03325

Alexander, M. J., Geller, M., McLandress, C., Polavarapu, S., Preusse, P., Sassi, F., … Watanabe, S. (2010). Recent developments in gravity-wave effects in climate models and the global distribution of gravity-wave momentum flux from observations and models. *Quarterly Journal of the Royal Meteorological Society*, *136*(650), 1103–1124. https://doi.org/10.1002/QJ.637

Alexander, S. P., Sato, K., Watanabe, S., Kawatani, Y., & Murphy, D. J. (2016). Southern Hemisphere Extratropical Gravity Wave Sources and Intermittency Revealed by a Middle-Atmosphere General Circulation Model. *Journal of the Atmospheric Sciences*, *73*(3), 1335–1349. https://doi.org/10.1175/JAS-D-15-0149.1

Allen, D. R., Bevilacqua, R. M., Nedoluha, G. E., Randall, C. E., & Manney, G. L. (2003). Unusual stratospheric transport and mixing during the 2002 Antarctic winter. *Geophysical Research Letters*, *30*(12). https://doi.org/10.1029/2003GL017117

Allen, D. R., & Nakamura, N. (2002). Dynamical reconstruction of the record low column ozone over Europe on 30 November 1999. *Geophysical Research Letters*, *29*(9), 76-1-76–4. https://doi.org/10.1029/2002GL014935

Andrews, D. G., Holton, J. R., & Leovy, C. B. (1987). *Middle atmosphere dynamics No. 40*. Academic press.

Atlas, D., Metcalf, J. I., Richter, J. H., & Gossard, E. E. (1970). The Birth of "CAT" and Microscale Turbulence. *Journal of the Atmospheric Sciences*, *27*(6), 903–913.

Becker, E. (2009). Sensitivity of the Upper Mesosphere to the Lorenz Energy Cycle of the

Troposphere. *Journal of the Atmospheric Sciences*, *66*(3), 647–666. https://doi.org/10.1175/2008JAS2735.1

Birner, T., & Bönisch, H. (2011). Residual circulation trajectories and transit times into the extratropical lowermost stratosphere. *Atmospheric Chemistry and Physics*, *11*(2), 817–827. https://doi.org/10.5194/ACP-11-817-2011

Birner, T., Sankey, D., & Shepherd, T. G. (2006). The tropopause inversion layer in models and analyses. *Geophysical Research Letters*, *33*(14). https://doi.org/10.1029/2006GL026549

Blumen, W., Banta, R. M., Burns, S. P., Fritts, D. C., Newsom, R. K., Poulos, G. S., & Sun, J. (2001). Turbulence statistics of a Kelvin–Helmholtz billow event observed in the night-time boundary layer during the Cooperative Atmosphere–Surface Exchange Study field program. *Dynamics of Atmospheres and Oceans*, *34*(2–4), 189–204. https://doi.org/10.1016/S0377-0265(01)00067-7

Browning, K. A., & Watkins, C. D. (1970). Observations of Clear Air Turbulence by High Power Radar. *Nature 1970 227:5255*, *227*(5255), 260–263. https://doi.org/10.1038/227260a0

Butchart, N. (2014). The Brewer-Dobson circulation. *Reviews of Geophysics*, *52*(2), 157–184. https://doi.org/10.1002/2013RG000448

Butler, A. H., & Gerber, E. P. (2018). Optimizing the Definition of a Sudden Stratospheric Warming. *Journal of Climate*, *31*(6), 2337–2344. https://doi.org/10.1175/JCLI-D-17-0648.1

Butler, A. H., Seidel, D. J., Hardiman, S. C., Butchart, N., Birner, T., & Match, A. (2015). Defining Sudden Stratospheric Warmings. *Bulletin of the American Meteorological Society*, *96*(11), 1913–1928. https://doi.org/10.1175/BAMS-D-13-00173.1

Chapman, D., & Browning, K. A. (1999). Release of potential shearing instability in warm frontal zones. *Quarterly Journal of the Royal Meteorological Society*, *125*(558), 2265–2289. https://doi.org/10.1002/QJ.49712555815

Charney, J. G., & Drazin, P. G. (1961). Propagation of planetary-scale disturbances from the lower into the upper atmosphere. *Journal of Geophysical Research*, *66*(1), 83–109. https://doi.org/10.1029/JZ066I001P00083

Chilson, P. B., Muschinski, A., & Schmidt, G. (1997). First observations of Kelvin-Helmholtz billows in an upper level jet stream using VHF frequency domain interferometry. *Radio Science*, *32*(3), 1149–1160. https://doi.org/10.1029/97RS00088

Cronenwett, W. T., Walker, G. B., & Inman, R. L. (1972). Acoustic Sounding of Meteorological Phenomena in the Planetary Boundary Layer. *Journal of Applied Meteorology and Climatology*, *11*(8), 1351–1358.

Emmanuel, C. B., Bean, B. R., McAllister, L. G., & Pollard, J. R. (1972). Observations of Helmholtz Waves in the Lower Atmosphere with an Acoustic Sounder. *Journal of the Atmospheric Sciences*, *29*(5), 886–892.

Ern, M., Trinh, Q. T., Preusse, P., Gille, J. C., Mlynczak, M. G., Iii, J. M. R., & Riese, M. (2018). GRACILE: A comprehensive climatology of atmospheric gravity wave parameters based on satellite limb soundings. *Earth System Science Data*, *10*(2), 857–892. https://doi.org/10.5194/ESSD-10-857-2018

Ern, M., Preusse, P., Alexander, M. J., & Warner, C. D. (2004). Absolute values of gravity wave momentum flux derived from satellite data. *Journal of Geophysical Research: Atmospheres*, *109*(D20), 20103. https://doi.org/10.1029/2004JD004752

Fritts, D. C. (1979). *The Excitation of Radiating Waves and Kelvin-Helmholtz Instabilities by the Gravity Wave-Critical Level Interaction*. *Journal of the Atmospheric Sciences* (Vol. 36). American Meteorological Society. https://doi.org/10.1175/1520-0469(1979)036<0012:TEORWA>2.0.CO;2

Fritts, D. C., & Alexander, M. J. (2003). Gravity wave dynamics and effects in the middle

atmosphere. *Reviews of Geophysics*, *41*(1). https://doi.org/10.1029/2001RG000106

Fukao, S., & Hamazu, K. (2014). Radar for meteorological and atmospheric observations. *Radar for Meteorological and Atmospheric Observations*, *9784431543*, 1–537. https://doi.org/10.1007/978-4-431-54334-3

Fukao, S., Luce, H., Mega, T., & Yamamoto, M. (2011). Extensive studies of large-amplitude Kelvin–Helmholtz billows in the lower atmosphere with VHF middle and upper atmosphere radar. *Quarterly Journal of the Royal Meteorological Society*, *137*(657), 1019–1041. https://doi.org/10.1002/QJ.807

Garcia, R. R., Lieberman, R. S., Russell, J. M., & Mlynczak, M. G. (2005). Large-Scale Waves in the Mesosphere and Lower Thermosphere Observed by SABER. *Journal of the Atmospheric Sciences*, *62*(12), 4384–4399. https://doi.org/10.1175/JAS3612.1

Geerts, B., Miao, Q., Yang, Y., Rasmussen, R., & Breed, D. (2010). An Airborne Profiling Radar Study of the Impact of Glaciogenic Cloud Seeding on Snowfall from Winter Orographic Clouds. *Journal of the Atmospheric Sciences*, *67*(10), 3286–3302. https://doi.org/10.1175/2010JAS3496.1

Geerts, B., Damiani, R., & Haimov, S. (2006). Finescale Vertical Structure of a Cold Front as Revealed by an Airborne Doppler Radar. *Monthly Weather Review*, *134*(1), 251–271. https://doi.org/10.1175/MWR3056.1

Gelaro, R., McCarty, W., Suárez, M. J., Todling, R., Molod, A., Takacs, L., … Zhao, B. (2017). The Modern-Era Retrospective Analysis for Research and Applications, Version 2 (MERRA-2). *Journal of Climate*, *30*(14), 5419–5454. https://doi.org/10.1175/JCLI-D-16-0758.1

Gossard, E. E., Richter, J. H., & Atlas, D. (1970). Internal waves in the atmosphere from high-resolution radar measurements. *Journal of Geophysical Research*, *75*(18), 3523–3536. https://doi.org/10.1029/JC075I018P03523

Grasmick, C., & Geerts, B. (2020). Detailed Dual-Doppler Structure of Kelvin–Helmholtz Waves from an Airborne Profiling Radar over Complex Terrain. Part I: Dynamic Structure. *Journal of the Atmospheric Sciences*, *77*(5), 1761–1782. https://doi.org/10.1175/JAS-D-19-0108.1

Grose, W. L., & Hoskins, B. J. (1979). On the Influence of Orography on Large-Scale Atmospheric Flow. *Journal of Atmospheric Sciences*, *36*(2), 223–234.

Hamilton, K., Wilson, R. J., & Hemler, R. S. (1999). Middle Atmosphere Simulated with High Vertical and Horizontal Resolution Versions of a GCM: Improvements in the Cold Pole Bias and Generation of a QBO-like Oscillation in the Tropics. *Journal of the Atmospheric Sciences*, *56*(22), 3829–3846. https://doi.org/10.1175/1520-0469(1999)056<3829:MASWHV>2.0.CO;2

Hardy, K. R., Reed, R. J., & Mather, G. K. (1973). Observation of Kelvin-Helmholtz billows and their mesoscale environment by radar, instrumented aircraft, and a dense radiosonde network. *Quarterly Journal of the Royal Meteorological Society*, *99*(420), 279–293. https://doi.org/10.1002/QJ.49709942007

Hertzog, A., Alexander, M. J., & Plougonven, R. (2012). On the intermittency of gravity wave momentum flux in the stratosphere. *Journal of the Atmospheric Sciences*, *69*(11), 3433–3448. https://doi.org/10.1175/JAS-D-12-09.1

Hertzog, A., Cocquerez, P., Basdevant, C., Boccara, G., Bordereau, J., Brioit, B., … Vial, F. (2007). Stratéole/Vorcore - Long-duration, superpressure balloons to study the Antarctic lower stratosphere during the 2005 winter. *Journal of Atmospheric and Oceanic Technology*, *24*(12), 2048–2061. https://doi.org/10.1175/2007JTECHA948.1

Hicks, J. J., & Angell, J. K. (1968). Radar Observations of Breaking Gravitational Waves in the Visually Clear Atmosphere. *Journal of Applied Meteorology and Climatology*, *7*(1), 114–121.

Hirooka, T., & Hirota, I. (1985). Normal Mode Rossby Waves Observed in the Upper Stratosphere. Part II: Second Antisymmetric and Symmetric Modes of Zonal Wavenumbers 1 and 2.

Journal of Atmospheric Sciences, *42*(6), 536–548. https://doi.org/10.1175/1520-0469(1985)042<0536:NMRWOI>2.0.CO;2

Hirota, I., Hirooka, T., & Shiotani, M. (1983). Upper stratospheric circulations in the two hemispheres observed by satellites. *Quarterly Journal of the Royal Meteorological Society*, *109*(461), 443–454. https://doi.org/10.1002/QJ.49710946102

Hocking, W. K. (1983). On the extraction of atmospheric turbulence parameters from radar backscatter Doppler spectra—I. Theory. *Journal of Atmospheric and Terrestrial Physics*, *45*(2–3), 89–102. https://doi.org/10.1016/S0021-9169(83)80013-0

Hocking, W. K. (1999). The dynamical parameters of turbulence theory as they apply to middle atmosphere studies. *Earth, Planets and Space*, *51*(7–8), 525–541. https://doi.org/10.1186/BF03353213/METRICS

Hoffmann, P., Becker, E., Singer, W., & Placke, M. (2010). Seasonal variation of mesospheric waves at northern middle and high latitudes. *Journal of Atmospheric and Solar-Terrestrial Physics*, *72*(14–15), 1068–1079. https://doi.org/10.1016/J.JASTP.2010.07.002

Holton, J. R. (1983). The Influence of Gravity Wave Breaking on the General Circulation of the Middle Atmosphere. *Journal of the Atmospheric Sciences*, *40*(10), 2497–2507. https://doi.org/10.1175/1520-0469(1983)040

Hoskins, B. J., & Karoly, D. J. (1981). The Steady Linear Response of a Spherical Atmosphere to Thermal and Orographic Forcing. *Journal of Atmospheric Sciences*, *38*(6), 1179–1196. Retrieved from https://www.webofscience.com/wos/woscc/full-record/WOS:A1981MC11400005

Jin, H., Miyoshi, Y., Fujiwara, H., Shinagawa, H., Terada, K., Terada, N., … Saito, A. (2011). Vertical connection from the tropospheric activities to the ionospheric longitudinal structure simulated by a new Earth's whole atmosphere-ionosphere coupled model. *Journal of*

Geophysical Research: Space Physics, *116*(A1), 1316. https://doi.org/10.1029/2010JA015925

Kantha, L., Lawrence, D., Luce, H., Hashiguchi, H., Tsuda, T., Wilson, R. J., … Yabuki, M. (2017). Shigaraki UAV-Radar Experiment (ShUREX): overview of the campaign with some preliminary results. *Progress in Earth and Planetary Science*, *4*(1), 1–26. https://doi.org/10.1186/S40645-017-0133-X/FIGURES/23

Klostermeyer, J., & Rüster, R. (1980). Radar observation and model computation of a jet stream-generated Kelvin-Helmholtz instability. *Journal of Geophysical Research: Oceans*, *85*(C5), 2841–2846. https://doi.org/10.1029/JC085IC05P02841

Kodera, K. (2006). Influence of stratospheric sudden warming on the equatorial troposphere. *Geophysical Research Letters*, *33*(6). https://doi.org/10.1029/2005GL024510

Kohma, M., & Sato, K. (2014). Variability of upper tropospheric clouds in the polar region during stratospheric sudden warmings. *Journal of Geophysical Research: Atmospheres*, *119*(17), 10,100-10,113. https://doi.org/10.1002/2014JD021746

Kohma, M., Sato, K., Tomikawa, Y., Nishimura, K., & Sato, T. (2019). Estimate of Turbulent Energy Dissipation Rate From the VHF Radar and Radiosonde Observations in the Antarctic. *Journal of Geophysical Research: Atmospheres*, *124*(6), 2976–2993. https://doi.org/10.1029/2018JD029521

Kohma, M., Sato, K., Nishimura, K., Tsutsumi, M., & Sato, T. (2020). A Statistical Analysis of the Energy Dissipation Rate Estimated From the PMWE Spectral Width in the Antarctic. *Journal of Geophysical Research: Atmospheres*, *125*(16), e2020JD032745. https://doi.org/10.1029/2020JD032745

Koshin, D., Sato, K., Miyazaki, K., & Watanabe, S. (2020). An ensemble Kalman filter data assimilation system for the whole neutral atmosphere. *Geoscientific Model Development*, *13*(7), 3145–3177. https://doi.org/10.5194/GMD-13-3145-2020

Koshin, D., Sato, K., Kohma, M., & Watanabe, S. (2021). An update on the 4D-LETKF data assimilation system for the whole neutral atmosphere. *Geoscientific Model Development Discussions*, 1–25. https://doi.org/10.5194/GMD-2020-381

Lait, L. R. (1994). An Alternative Form for Potential Vorticity. *Journal of Atmospheric Sciences*, *51*(12), 1754–1759. https://doi.org/10.1175/1520-0469(1994)051<1754:AAFFPV>2.0.CO;2

Lawrence, B. N., & Randel, W. J. (1996). Variability in the mesosphere observed by the Nimbus 6 pressure modulator radiometer. *Journal of Geophysical Research: Atmospheres*, *101*(D18), 23475–23489. https://doi.org/10.1029/96JD01652

Lieberman, R. S., Riggin, D. M., Franke, S. J., Manson, A. H., Meek, C., Nakamura, T., … Reid, I. M. (2003). The 6.5-day wave in the mesosphere and lower thermosphere: Evidence for baroclinic/barotropic instability. *Journal of Geophysical Research: Atmospheres*, *108*(D20), 4640. https://doi.org/10.1029/2002JD003349

Lim, E. P., Hendon, H. H., Butler, A. H., Garreaud, R. D., Polichtchouk, I., Shepherd, T. G., … Newman, P. A. (2020). The 2019 Antarctic sudden stratospheric warming. *SPARC Newsletter*, *54*, 10–13.

Limpasuvan, V., Orsolini, Y. J., Chandran, A., Garcia, R. R., & Smith, A. K. (2016). On the composite response of the MLT to major sudden stratospheric warming events with elevated stratopause. *Journal of Geophysical Research: Atmospheres*, *121*(9), 4518–4537. https://doi.org/10.1002/2015JD024401

Lin, P., & Fu, Q. (2013). Changes in various branches of the Brewer–Dobson circulation from an ensemble of chemistry climate models. *Journal of Geophysical Research: Atmospheres*, *118*(1), 73–84. https://doi.org/10.1029/2012JD018813

Liu, H. L., McInerney, J. M., Santos, S., Lauritzen, P. H., Taylor, M. A., & Pedatella, N. M. (2014). Gravity waves simulated by high-resolution Whole Atmosphere Community Climate Model.

Geophysical Research Letters, *41*(24), 9106–9112. https://doi.org/10.1002/2014GL062468

Liu, H. L., Talaat, E. R., Roble, R. G., Lieberman, R. S., Riggin, D. M., & Yee, J. H. (2004). The 6.5-day wave and its seasonal variability in the middle and upper atmosphere. *Journal of Geophysical Research: Atmospheres*, *109*(D21), 21112. https://doi.org/10.1029/2004JD004795

Luce, H., Yamamoto, M., Fukao, S., Helal, D., & Crochet, M. (2001). A frequency domain radar interferometric imaging (FII) technique based on high-resolution methods. *Journal of Atmospheric and Solar-Terrestrial Physics*, *63*(2–3), 221–234. https://doi.org/10.1016/S1364-6826(00)00147-4

Luce, H., Kantha, L., Hashiguchi, H., Lawrence, D., & Doddi, A. (2018). Turbulence kinetic energy dissipation rates estimated from concurrent UAV and MU radar measurements. *Earth, Planets and Space*, *70*(1), 1–19. https://doi.org/10.1186/S40623-018-0979-1/FIGURES/15

Luce, H., Hassenpflug, G., Yamamoto, M., & Fukao, S. (2006). High-resolution vertical imaging of the troposphere and lower stratosphere using the new MU radar system. *Annales Geophysicae*, *24*(3), 791–805. https://doi.org/10.5194/ANGEO-24-791-2006

Luce, H., Hassenpflug, G., Yamamoto, M., Crochet, M., & Fukao, S. (2007). Range-imaging observations of cumulus convection and Kelvin-Helmholtz instabilities with the MU radar. *Radio Science*, *42*(1), n/a-n/a. https://doi.org/10.1029/2005RS003439

Luce, H., Hassenpflug, G., Yamamoto, M., Fukao, S., & Sato, K. (2008). High-Resolution Observations with MU Radar of a KH Instability Triggered by an Inertia–Gravity Wave in the Upper Part of a Jet Stream. *Journal of the Atmospheric Sciences*, *65*(5), 1711–1718. https://doi.org/10.1175/2007JAS2346.1

Mahalov, A., Moustaoui, M., Nicolaenko, B., & Tse, K. L. (2007). Computational studies of inertia-gravity waves radiated from upper tropospheric jets. *Theoretical and Computational Fluid*

Dynamics 2007 21:6, *21*(6), 399–422. https://doi.org/10.1007/S00162-007-0062-1

Manney, G. L., Schwartz, M. J., Krüger, K., Santee, M. L., Pawson, S., Lee, J. N., … Livesey, N. J. (2009). Aura Microwave Limb Sounder observations of dynamics and transport during the record-breaking 2009 Arctic stratospheric major warming. *Geophysical Research Letters*, *36*(12). https://doi.org/10.1029/2009GL038586

Matsuno, T. (1971). A Dynamical Model of the Stratospheric Sudden Warming. *Journal of Atmospheric Sciences*, *28*(8), 1479–1494. https://doi.org/10.1175/1520-0469(1971)028<1479:ADMOTS>2.0.CO;2

Medina, S., & Houze, R. A. (2016). Kelvin–Helmholtz waves in extratropical cyclones passing over mountain ranges. *Quarterly Journal of the Royal Meteorological Society*, *142*(696), 1311–1319. https://doi.org/10.1002/QJ.2734

Meyer, C. K., & Forbes, J. M. (1997). A 6.5-day westward propagating planetary wave: Origin and characteristics. *Journal of Geophysical Research: Atmospheres*, *102*(D22), 26173–26178. https://doi.org/10.1029/97JD01464

Miles, J. W., & Howard, L. N. (1964). Note on a heterogeneous shear flow. *Journal of Fluid Mechanics*, *20*(2), 331–336. https://doi.org/10.1017/S0022112064001252

Minamihara, Y., Sato, K., Tsutsumi, M., & Sato, T. (2018). Statistical Characteristics of Gravity Waves With Near-Inertial Frequencies in the Antarctic Troposphere and Lower Stratosphere Observed by the PANSY Radar. *Journal of Geophysical Research: Atmospheres*, *123*(17), 8993–9010. https://doi.org/10.1029/2017JD028128

Minamihara, Y., Sato, K., & Tsutsumi, M. (2020). Intermittency of Gravity Waves in the Antarctic Troposphere and Lower Stratosphere Revealed by the PANSY Radar Observation. *Journal of Geophysical Research: Atmospheres*, *125*(15), e2020JD032543. https://doi.org/10.1029/2020JD032543

Minamihara, Y., Sato, K., Kohma, M., & Tsutsumi, M. (2016). Characteristics of vertical wind fluctuations in the lower troposphere at syowa station in the antarctic revealed by the PANSY radar. *Scientific Online Letters on the Atmosphere*, *12*, 116–120. https://doi.org/10.2151/sola.2016-026

Nastrom, G. D., & Eaton, F. D. (1997). Turbulence eddy dissipation rates from radar observations at 5–20 km at White Sands Missile Range, New Mexico. *Journal of Geophysical Research: Atmospheres*, *102*(D16), 19495–19505. https://doi.org/10.1029/97JD01262

Newsom, R. K., & Banta, R. M. (2003). Shear-Flow Instability in the Stable Nocturnal Boundary Layer as Observed by Doppler Lidar during CASES-99. *Journal of the Atmospheric Sciences*, *60*(1), 16–33. https://doi.org/10.1175/1520-0469(2003)060

Nishimura, K., Kohma, M., Sato, K., & Sato, T. (2020). Spectral Observation Theory and Beam Debroadening Algorithm for Atmospheric Radar. *IEEE Transactions on Geoscience and Remote Sensing*, *58*(10), 6767–6775. https://doi.org/10.1109/TGRS.2020.2970200

Okamoto, K., Sato, K., & Akiyoshi, H. (2011). A study on the formation and trend of the Brewer-Dobson circulation. *Journal of Geophysical Research: Atmospheres*, *116*(D10). https://doi.org/10.1029/2010JD014953

Okui, H., Sato, K., Koshin, D., & Watanabe, S. (2021). Formation of a Mesospheric Inversion Layer and the Subsequent Elevated Stratopause Associated With the Major Stratospheric Sudden Warming in 2018/19. *Journal of Geophysical Research: Atmospheres*, *126*(18). https://doi.org/10.1029/2021JD034681

Onogi, K., Tsutsui, J., Koide, H., Sakamoto, M., Kobayashi, S., Hatsushika, H., … Taira, R. (2007). The JRA-25 Reanalysis. *Journal of the Meteorological Society of Japan. Ser. II*, *85*(3), 369–432. https://doi.org/10.2151/JMSJ.85.369

Palmer, R. D., Yu, T. Y., & Chilson, P. B. (1999). Range imaging using frequency diversity. *Radio*

Science, *34*(6), 1485–1496. https://doi.org/10.1029/1999RS900089

Petre, J. M., & Verlinde, J. (2004). Cloud Radar Observations of Kelvin–Helmholtz Instability in a Florida Anvil. *Monthly Weather Review*, *132*(10), 2520–2523.

Plougonven, R., Hertzog, A., & Guez, L. (2013). Gravity waves over Antarctica and the Southern Ocean: consistent momentum fluxes in mesoscale simulations and stratospheric balloon observations. *Quarterly Journal of the Royal Meteorological Society*, *139*(670), 101–118. https://doi.org/10.1002/QJ.1965

Plougonven, R., & Zhang, F. (2014). Internal gravity waves from atmospheric jets and fronts. *Reviews of Geophysics*, *52*(1), 33–76. https://doi.org/10.1002/2012RG000419

Plumb, R. A. (1983). Baroclinic Instability of the Summer Mesosphere: A Mechanism for the Quasi-Two-Day Wave? *Journal of Atmospheric Sciences*, *40*(1), 262–270. https://doi.org/10.1175/1520-0469(1983)040<0262:BIOTSM>2.0.CO;2

Plumb, R. A. (2002). Stratospheric Transport. *Journal of the Meteorological Society of Japan. Ser. II*, *80*(4B), 793–809. https://doi.org/10.2151/JMSJ.80.793

Preusse, P., Eckermann, S. D., & Ern, M. (2008). Transparency of the atmosphere to short horizontal wavelength gravity waves. *Journal of Geophysical Research: Atmospheres*, *113*(D24), 24104. https://doi.org/10.1029/2007JD009682

Preusse, P., Dörnbrack, A., Eckermann, S. D., Riese, M., Schaeler, B., Bacmeister, J. T., … Grossmann, K. U. (2002). Space-based measurements of stratospheric mountain waves by CRISTA 1. Sensitivity, analysis method, and a case study. *Journal of Geophysical Research: Atmospheres*, *107*(D23), CRI 6-1. https://doi.org/10.1029/2001JD000699

Rabier, F., Bouchard, A., Brun, E., Doerenbecher, A., Guedj, S., Guidard, V., … Steinle, P. (2010). The Concordiasi Project in Antarctica. *Bulletin of the American Meteorological Society*, *91*(1), 69–86. https://doi.org/10.1175/2009BAMS2764.1

Ralph, F. M., Neiman, P. J., Keller, T. L., Levinson, D., & Fedor, L. (1997). Observations, Simulations, and Analysis of Nonstationary Trapped Lee Waves. *Journal of the Atmospheric Sciences*, *54*(10), 1308–1333. https://doi.org/10.1175/1520-0469(1997)054

Reichler, T., Kim, J., Manzini, E., & Kröger, J. (2012). A stratospheric connection to Atlantic climate variability. *Nature Geoscience 2012 5:11*, *5*(11), 783–787. https://doi.org/10.1038/ngeo1586

Salby, M. L. (1981). Rossby Normal Modes in Nonuniform Background Configurations. Part I: Simple Fields. *Journal of Atmospheric Sciences*, *38*(9), 1803–1826. https://doi.org/10.1175/1520-0469(1981)038<1803:RNMINB>2.0.CO;2

Samelson, R. M., & Skyllingstad, E. D. (2016). Frontogenesis and Turbulence: A Numerical Simulation. *Journal of the Atmospheric Sciences*, *73*(12), 5025–5040. https://doi.org/10.1175/JAS-D-16-0145.1

Sassen, K. (2002). Indirect climate forcing over the western US from Asian dust storms. *Geophysical Research Letters*, *29*(10), 103-1-103–4. https://doi.org/10.1029/2001GL014051

Sato, K. (1994). A statistical study of the structure, saturation and sources of inertio-gravity waves in the lower stratosphere observed with the MU radar. *Journal of Atmospheric and Terrestrial Physics*, *56*(6), 755–774. https://doi.org/10.1016/0021-9169(94)90131-7

Sato, K., O'Sullivan, D. J., & Dunkerton, T. J. (1997). Low-frequency inertia-gravity waves in the stratosphere revealed by three-week continuous observation with the MU radar. *Geophysical Research Letters*, *24*(14), 1739–1742. https://doi.org/10.1029/97GL01759

Sato, K., & Hirano, S. (2019). The climatology of the Brewer-Dobson circulation and the contribution of gravity waves. *Atmospheric Chemistry and Physics*, *19*(7), 4517–4539. https://doi.org/10.5194/ACP-19-4517-2019

Sato, K., Yasui, R., & Miyoshi, Y. (2018). The Momentum Budget in the Stratosphere,

Mesosphere, and Lower Thermosphere. Part I: Contributions of Different Wave Types and In Situ Generation of Rossby Waves. *Journal of the Atmospheric Sciences*, *75*(10), 3613–3633. https://doi.org/10.1175/JAS-D-17-0336.1

Sato, K., & Nomoto, M. (2015). Gravity Wave–Induced Anomalous Potential Vorticity Gradient Generating Planetary Waves in the Winter Mesosphere. *Journal of the Atmospheric Sciences*, *72*(9), 3609–3624. https://doi.org/10.1175/JAS-D-15-0046.1

Sato, K., Kohma, M., Tsutsumi, M., & Sato, T. (2017). Frequency spectra and vertical profiles of wind fluctuations in the summer Antarctic mesosphere revealed by MST radar observations. *Journal of Geophysical Research: Atmospheres*, *122*(1), 3–19. https://doi.org/10.1002/2016JD025834

Sato, K., Kumakura, T., & Takahashi, M. (1999). Gravity Waves Appearing in a High-Resolution GCM Simulation. *Journal of the Atmospheric Sciences*, *56*(8), 1005–1018. https://doi.org/10.1175/1520-0469(1999)056<1005:GWAIAH>2.0.CO;2

Sato, K., Watanabe, S., Kawatani, Y., Tomikawa, Y., Miyazaki, K., & Takahashi, M. (2009). On the origins of mesospheric gravity waves. *Geophysical Research Letters*, *36*(19). https://doi.org/10.1029/2009GL039908

Sato, K., Tsutsumi, M., Sato, T., Nakamura, T., Saito, A., Tomikawa, Y., … Yamanouchi, T. (2014). Program of the Antarctic Syowa MST/IS radar (PANSY). *Journal of Atmospheric and Solar-Terrestrial Physics*, *118*, 2–15. https://doi.org/10.1016/J.JASTP.2013.08.022

Sato, K., & Yoshiki, M. (2008). Gravity Wave Generation around the Polar Vortex in the Stratosphere Revealed by 3-Hourly Radiosonde Observations at Syowa Station. *Journal of the Atmospheric Sciences*, *65*(12), 3719–3735. https://doi.org/10.1175/2008JAS2539.1

Sato, T., & Woodman, R. F. (1982). Fine Altitude Resolution Observations of Stratospheric Turbulent Layers by the Arecibo 430 MHz Radar. *Journal of Atmospheric Sciences*, *39*(11),

2546–2552. https://doi.org/10.1175/1520-0469(1982)039<2546:FAROOS>2.0.CO;2

Satoh, M., Matsuno, T., Tomita, H., Miura, H., Nasuno, T., & Iga, S. (2008). Nonhydrostatic icosahedral atmospheric model (NICAM) for global cloud resolving simulations. *Journal of Computational Physics*, *227*(7), 3486–3514. https://doi.org/10.1016/J.JCP.2007.02.006

Satoh, M., Tomita, H., Yashiro, H., Miura, H., Kodama, C., Seiki, T., … Kubokawa, H. (2014). The Non-hydrostatic Icosahedral Atmospheric Model: description and development. *Progress in Earth and Planetary Science 2014 1:1*, *1*(1), 1–32. https://doi.org/10.1186/S40645-014-0018-1

Schneider, A., Gerding, M., & Lübken, F. J. (2015). Comparing turbulent parameters obtained from LITOS and radiosonde measurements. *Atmospheric Chemistry and Physics*, *15*(4), 2159–2166. https://doi.org/10.5194/ACP-15-2159-2015

Schoeberl, M. R., & Hartmann, D. L. (1991). The Dynamics of the Stratospheric Polar Vortex and Its Relation to Springtime Ozone Depletions. *Science*, *251*(4989), 46–52. https://doi.org/10.1126/science.251.4989.46

Scorer, R. S. (1969). *Billow mechanics* (Vol. 4). https://doi.org/10.1029/RS004i012p01299

Seviour, W. J. M., Butchart, N., & Hardiman, S. C. (2012). The Brewer–Dobson circulation inferred from ERA-Interim. *Quarterly Journal of the Royal Meteorological Society*, *138*(665), 878–888. https://doi.org/10.1002/QJ.966

Sha, W., Kawamura, T., & Ueda, H. (1991). A Numerical Study on Sea/Land Breezes as a Gravity Current: Kelvin–Helmholtz Billows and Inland Penetration of the Sea-Breeze Front. *Journal of Atmospheric Sciences*, *48*(14), 1649–1665. https://doi.org/10.1175/1520-0469(1991)048<1649:ANSOSB>2.0.CO;2

Shibuya, R., Sato, K., Tsutsumi, M., Sato, T., Tomikawa, Y., Nishimura, K., & Kohma, M. (2017). Quasi-12 h inertia-gravity waves in the lower mesosphere observed by the PANSY radar at

Syowa Station (39.6° E, 69.0° S). *Atmospheric Chemistry and Physics*, *17*(10), 6455–6476. https://doi.org/10.5194/ACP-17-6455-2017

Shibuya, R., & Sato, K. (2019). A study of the dynamical characteristics of inertia-gravity waves in the Antarctic mesosphere combining the PANSY radar and a non-hydrostatic general circulation model. *Atmospheric Chemistry and Physics*, *19*(5), 3395–3415. https://doi.org/10.5194/ACP-19-3395-2019

Shibuya, R., Miura, H., & Sato, K. (2016). A Grid Transformation Method for a Quasi-Uniform, Circular Fine Region Using the Spring Dynamics. *Journal of the Meteorological Society of Japan. Ser. II*, *94*(5), 2016–022. https://doi.org/10.2151/JMSJ.2016-022

Takayabu, I. (1992). Kelvin-Helmholtz Billow Clouds on a Frontal Surface. *Journal of the Meteorological Society of Japan. Ser. II*, *70*(2), 733–738. https://doi.org/10.2151/JMSJ1965.70.2_733

Talaat, E. R., Yee, J. H., & Zhu, X. (2002). The 6.5-day wave in the tropical stratosphere and mesosphere. *Journal of Geophysical Research: Atmospheres*, *107*(D12), ACL 1-1. https://doi.org/10.1029/2001JD000822

Theuerkauf, A., Gerding, M., & Lübken, F. J. (2011). LITOS - A new balloon-borne instrument for fine-scale turbulence soundings in the stratosphere. *Atmospheric Measurement Techniques*, *4*(1), 55–66. https://doi.org/10.5194/AMT-4-55-2011

Tomikawa, Y., Nomoto, M., Miura, H., Tsutsumi, M., Nishimura, K., Nakamura, T., … Sato, K. (2015). Vertical Wind Disturbances during a Strong Wind Event Observed by the PANSY Radar at Syowa Station, Antarctica. *Monthly Weather Review*, *143*(5), 1804–1821. https://doi.org/10.1175/MWR-D-14-00289.1

Tomikawa, Y., Sato, K., Watanabe, S., Kawatani, Y., Miyazaki, K., & Takahashi, M. (2012). Growth of planetary waves and the formation of an elevated stratopause after a major

stratospheric sudden warming in a T213L256 GCM. *Journal of Geophysical Research: Atmospheres*, *117*(D16), 16101. https://doi.org/10.1029/2011JD017243

Tomikawa, Y., Nishimura, Y., & Yamanouchi, T. (2009). Characteristics of Tropopause and Tropopause Inversion Layer in the Polar Region. *SOLA*, *5*(1), 141–144. https://doi.org/10.2151/SOLA.2009-036

Tomita, H., & Satoh, M. (2004). A new dynamical framework of nonhydrostatic global model using the icosahedral grid. *Fluid Dynamics Research*, *34*(6), 357–400. https://doi.org/10.1016/J.FLUIDDYN.2004.03.003/XML

Trier, S. B., Sharman, R. D., MuñOz-Esparza, D., & Lane, T. P. (2020). Environment and Mechanisms of Severe Turbulence in a Midlatitude Cyclone. *Journal of the Atmospheric Sciences*, *77*(11), 3869–3889. https://doi.org/10.1175/JAS-D-20-0095.1

Vallis, G. K. (2017). *Atmospheric and oceanic fluid dynamics*. Cambridge University Press.

VanLoon, H., Jenne, R. L., & Labitzke, K. (1973). Zonal harmonic standing waves. *Journal of Geophysical Research*, *78*(21), 4463–4471. https://doi.org/10.1029/JC078I021P04463

VanZandt, T. E., Green, J. L., Clark, W. L., & Grant, J. R. (1979). Buoyancy waves in the troposphere: Doppler radar observations and a theoretical model. *Geophysical Research Letters*, *6*(6), 429–432. https://doi.org/10.1029/GL006I006P00429

Vincent, R. A., & Reid, I. M. (1983). HF Doppler Measurements of Mesospheric Gravity Wave Momentum Fluxes. *Journal of Atmospheric Sciences*, *40*(5), 1321–1333. https://doi.org/10.1175/1520-0469(1983)040<1321:HDMOMG>2.0.CO;2

Wakimoto, R. M., Blier, W., & Liu, C. (1992). The Frontal Structure of an Explosive Oceanic Cyclone: Airbone Radar Observations of ERICA IOP 4. *Monthly Weather Review*, *120*(7), 1135–1155.

Watanabe, S., & Miyahara, S. (2009). Quantification of the gravity wave forcing of the migrating

diurnal tide in a gravity wave–resolving general circulation model. *Journal of Geophysical Research: Atmospheres*, *114*(D7), 7110. https://doi.org/10.1029/2008JD011218

Watanabe, S., Kawatani, Y., Tomikawa, Y., Miyazaki, K., Takahashi, M., & Sato, K. (2008). General aspects of a T213L256 middle atmosphere general circulation model. *Journal of Geophysical Research: Atmospheres*, *113*(D12), 12110. https://doi.org/10.1029/2008JD010026

Watanabe, S., Tomikawa, Y., Sato, K., Kawatani, Y., Miyazaki, K., & Takahashi, M. (2009). Simulation of the eastward 4-day wave in the Antarctic winter mesosphere using a gravity wave resolving general circulation model. *Journal of Geophysical Research: Atmospheres*, *114*(D16), 16111. https://doi.org/10.1029/2008JD011636

Watanabe, S., Sato, K., Kawatani, Y., & Takahashi, M. (2015). Vertical resolution dependence of gravity wave momentum flux simulated by an atmospheric general circulation model. *Geoscientific Model Development*, *8*(6), 1637–1644. https://doi.org/10.5194/GMD-8-1637-2015

Wu, D. L., Hays, P. B., & Skinner, W. R. (1994). Observations of the 5-day wave in the mesosphere and lower thermosphere. *Geophysical Research Letters*, *21*(24), 2733–2736. https://doi.org/10.1029/94GL02660

Yamazaki, Y., Matthias, V., Miyoshi, Y., Stolle, C., Siddiqui, T., Kervalishvili, G., … Alken, P. (2020). September 2019 Antarctic Sudden Stratospheric Warming: Quasi-6-Day Wave Burst and Ionospheric Effects. *Geophysical Research Letters*, *47*(1), e2019GL086577. https://doi.org/10.1029/2019GL086577

Yasui, R., Sato, K., & Miyoshi, Y. (2018). The Momentum Budget in the Stratosphere, Mesosphere, and Lower Thermosphere. Part II: The In Situ Generation of Gravity Waves. *Journal of the Atmospheric Sciences*, *75*(10), 3635–3651. https://doi.org/10.1175/JAS-D-17-

0337.1

Yasui, R., Sato, K., & Miyoshi, Y. (2021). Roles of Rossby Waves, Rossby–Gravity Waves, and Gravity Waves Generated in the Middle Atmosphere for Interhemispheric Coupling. *Journal of the Atmospheric Sciences*, *78*(12), 3867–3888. https://doi.org/10.1175/JAS-D-21-0045.1

Yoshiki, M., & Sato, K. (2000). A statistical study of gravity waves in the polar regions based on operational radiosonde data. *Journal of Geophysical Research: Atmospheres*, *105*(D14), 17995–18011. https://doi.org/10.1029/2000JD900204

Yoshiki, M., Kizu, N., & Sato, K. (2004). Energy enhancements of gravity waves in the Antarctic lower stratosphere associated with variations in the polar vortex and tropospheric disturbances. *Journal of Geophysical Research: Atmospheres*, *109*(D23), 1–12. https://doi.org/10.1029/2004JD004870